energies

MDPI

Article

A CVaR-Robust Risk Aversion Scheduling Model for Virtual Power Plants Connected with Wind-Photovoltaic-Hydropower-Energy Storage Systems, Conventional Gas Turbines and Incentive-Based Demand Responses

Liwei Ju [1,3,*], Peng Li [2], Qinliang Tan [1,4], Zhongfu Tan [1,4] and GejiriFu De [1,4]

1 Schoolof Economic and management, North China Electric Power University, Beijing 102206, China; tql@ncepu.edu.cn (Q.T.); tzhf@ncepu.edu.cn (Z.T.); dove@ncepu.edu.cn (G.D.)
2 State Grid Henan Economic Research Institute, Zhengzhou 450052, China; hdlp0830@163.com
3 Beijing Energy Development Research Base, Beijing 102206, China
4 Beijing Key Laboratory of New Energy and Low-Carbon Development (North China Electric Power University), Changping District, Beijing 102206, China
* Correspondence: hdlwj@ncepu.edu.cn; Tel.: +86-176-0016-0816

Received: 13 September 2018; Accepted: 17 October 2018; Published: 25 October 2018

Abstract: To make full use of distributed energy resources to meet load demand, this study aggregated wind power plants (WPPs), photovoltaic power generation (PV), small hydropower stations (SHSs), energy storage systems (ESSs), conventional gas turbines (CGTs) and incentive-based demand responses (IBDRs) into a virtual power plant (VPP) with price-based demand response (PBDR). Firstly, a basic scheduling model for the VPP was proposed in this study with the objective of the maximum operation revenue. Secondly, a risk aversion model for the VPP was constructed based on the conditional value at risk (CVaR) method and robust optimization theory considering the operating risk from WPP and PV. Thirdly, a solution methodology was constructed and three cases were considered for comparative analyses. Finally, an independent micro-grid on an industrial park in East China was utilized for an example analysis. The results show the following: (1) the proposed risk aversion scheduling model could cope with the uncertainty risk via a reasonable confidence degree β and robust coefficient Γ. When $\Gamma \leq 0.85$ or $\Gamma \geq 0.95$, a small uncertainty brought great risk, indicating that the risk attitude of the decision maker will affect the scheduling scheme of the VPP, and the decision maker belongs to the risk extreme aversion type. When $\Gamma \in (0.85, 0.95)$, the decision-making scheme was in a stable state, the growth of β lead to the increase of CVaR, but the magnitude was not large. When the prediction error e was higher, the value of CVaR increased more when Γ increased by the same magnitude, which indicates that a lower prediction accuracy will amplify the uncertainty risk. (2) when the capacity ratio of (WPP, PV): ESS was higher than 1.5:1 and the peak-to-valley price gap was higher than 3:1, the values of revenue, VaR, and CVaR changed slower, indicating that both ESS and PBDR can improve the operating revenue, but the capacity scale of ESS and the peak-valley price gap need to be set properly, considering both economic benefits and operating risks. Therefore, the proposed risk aversion model could maximize the utilization of clean energy to obtain higher economic benefits while rationally controlling risks and provide reliable decision support for developing optimal operation plans for the VPP.

Keywords: risk aversion; dynamic scheduling; VPP; CVaR; robust optimization

1. Introduction

In recent years, under the dual pressures of energy shortages and environmental degradation, the development scale of distributed energy resources has gradually expanded, and its position in the energy grid has become increasingly prominent. However, due to their own limitations, the geographical distribution of the generators is dispersed, the unit capacity is small, and the intermittent fluctuation is obvious, so the direct grid connections of distributed energy resource (DER) units will have a great impact on the security and stability of the grid [1]. Therefore, researching flexible, safe, and reliable DER control technology is of great significance for realizing the large-scale grid connections of distributed energy. At present, China uses micro-grids to coordinate the operations of distributed power sources and loads [2], which effectively solves the technical contradictions between the grid and DERs. However, the main control target of a micro-grid is the local application of distributed power sources, which limits the effective utilization of multi-region and large-scale DERs. Virtual power plant (VPP) technology is a typical representation. Through advanced information technology, a large number of distributed power sources, controlled loads, and energy storage units are aggregated, realizing wide-area energy interconnection and sharing [3]. In particular, the rapid development of smart grid technologies promotes reasonable resource configurations and provides steady support for VPP operation.

Recently, the concept of VPP technology has attracted extensive attention in many industries, both domestically and internationally. In foreign countries, from 2001 to 2005, Germany, The Netherlands, and Spain jointly established the virtual fuel cell power plant program, consisting of 31 residential fuel cell combined heat and power (CHP) systems [4]. From 2005 to 2009, the United Kingdom, Spain, and France established a flexible electricity network in order to integrate the expected energy solution (FENIX) project [5] for the sustainable development of the EU power supply. The Netherlands established a power matching device VPP project consisting of 10 CHP units [6]. Cassell University integrated wind turbine, solar photovoltaic system, biogas power station and hydro power plant into VPP [7]. From 2009 to 2015, Denmark and Germany established electric vehicles in a distributed and integrated market using a sustainable energy and open networks (EDISON) project [8]. The EU completed the Web2Energy project and implemented the "Intelligent Power Distribution" project [9]. In China, in 2011, Zhang Bei, a new energy comprehensive utilization platform integrating wind power, photovoltaic power generation, energy storage and intelligent power transmission was put into production [10]. In 2014, the Xiaozhongdian distributed power demonstration project of the Guodian Group in Yunnan was successfully integrated into the Southern Power Grid [11]. In 2017, Xiong'an new district proposed a multi-energy source complementary scheme, which integrated medium-deep geothermal energy, shallow geothermal energy, and the waste heat from regenerated water and waste generation [12]. The "source-grid-load smart grid" system for the large-scale consumption of clean energy was first put into operation in Jiangsu [13]. In 2018, the commercial building VPP in Shanghai's Huangpu District was put into operation assembled from numerous distributed energy storage sources [14].

At present, studies on VPP operation optimization mainly focus on three aspects: the capacity allocation, optimization scheduling, and uncertainty handle. In terms of capacity allocation, Muhammad et al. [15] conducted a capacity allocation for a wind/firewood/storage/biomass independent micro-grid system by considering the net load fluctuations at different time scales. Aboelsood et al. [16] integrated a wind power plant (WPP), solar collectors, combined heat and power generation, and an energy storage system (ESS) to get the optimal operation cost. Bai et al. [17] proposed a multi-target capacity allocation optimization model for a wind/light/firewood/storage micro-grid system with a seawater desalination load with the objective of a minimum investment operation cost and a maximum renewable energy utilization ratio. Cao et al. [18] analyzed a micro-grid including renewable energy, energy storage, CHP system, etc., and the optimal outputs for each unit. Liu et al. [19] expressed the uncertainty of a wind power output by interval, and studied the robust stochastic bidding model for virtual power plants with wind/pumped storage/gas units. Faeze et al. [20] comprehensively

considered electrical energy storage, thermal energy storage, electric vehicles, and other resources to dispatch regional electric-thermal systems.

Research on the optimization scheduling of VPP operation focuses on the economic value and the elimination of wind and photovoltaic power as the objective to optimize the output of each unit in the dispatching system. Mashhour et al. [21] studied the bidding model of a VPP in the energy and rotating reserve market. Tascikaraoglu et al. [22] evaluated a virtual power plant strategy, including a hybrid system consisting of wind, solar, hydrogen, and thermal power systems. Mohammadi et al. [23] considered the complementarity and operational characteristics of wind, solar, and hydrogen, and studied a synergistic scheduling model of virtual power plants with the objective of maximum revenue. Shayeghi et al. [24] presented an optimal integrated participation model of wind and photovoltaic power generation (PV) energy, including storage devices and dispatchable distributed generation to increase their revenues. Shropshire et al. [25] constructed an optimal scheduling model of a virtual power plant including offshore wind farms and small nuclear power plants. Riveros et al. [26] presented a methodology to evaluate the optimal bidding strategy of a VPP coupled with district heating and renewable energy sources.

Finally, researches on the power fluctuation of VPP operation focus on how to use the controllable units, energy storage, electric vehicles and controllable loads to ensure the stable output of a VPP. Hrvoje et al. [27] have casted a two-stage stochastic model with uncertain parameters, including the power output of the intermittent source and the market prices. Heredia et al. [28] studied the bidding strategy of a VPP in the electricity market, and used the scene set to deal with the uncertainty of the market electricity price. Peik-Herfeh et al. [29] used a two-point estimation method to characterize the output fluctuation of the unit, which took two estimated points on both sides of the predicted value. Yang et al. [30] obtained wind speed distribution parameters by using a maximum likelihood estimation based on the characteristics of the wind speed, which obey the Weibull distribution. Zamani et al. [31] used the point estimation method to simulate uncertainties in the load and the renewable energy intermittent output in VPP scheduling. Tan et al. [32] established an economic dispatch model that considers the fluctuations in a renewable energy output based on chance constrained programming. Morteza et al. [33] used stochastic programming to deal with the uncertainty of electricity prices and proposed a VPP bidding model.

The optimization problem for VPP operation has been extensively discussed in all of the aforementioned studies. A capacity allocation method, scheduling model, and uncertainty handle technology have been proposed, which could greatly promote development. However, it should be noted that there are some gaps in the literatures. Firstly, most of the studies aggregated WPP, PV, ESS and conventional gas turbines (CGTs) into a VPP, and established a capacity allocation scheme, but for distributed power sources, small hydropower stations (SHSs), especially those with regulatory reservoirs, have a better application space for VPP. Secondly, the researches on the operation optimization of VPPs discussed the optimal operation strategies under different objective functions and different scenarios. Some studies considered the optimization effects of demand response on VPP. However, ESS and price-based demand response (PBDR) will flatten the load demand curve, which plays an important role in optimizing the VPP operation. It needs to be further discussed. Finally, some literatures studied the risks brought about by uncertainty. More studies used probabilistic methods to characterize uncertainty, but whether the DERs, whose capacity is small and quantity is large, have statistical properties remains to be verified, and probability distribution functions is difficult. In addition, uncertainty processing mainly relies on the stochastic programming method, which considers the probability distribution of uncertain factors, but the distribution law is difficult to describe. However, the optimal solution of robust optimization has certain inhibitions on the possible adverse effects of each element in the set. Adjusting the robust coefficient can decide the optimal scheduling schemes of different uncertainty degrees. This method does not need to consider numerous random schemes, so the calculation burden is small, and the applicable space is better. All of the above

analyses motivate us to propose an optimization scheduling model of a VPP. The main contributions of this work are summarized as follows:

- A VPP coupled with WPP, PV, SHS, ESS, CGT, and an incentive-based demand response (IBDR) with the implementation of PBDR on the user side. Among these, the SHS equipped with regulating reservoirs can distribute the output according to the real-time load demand, which can provide reserve services for the WPP and PV coupling operation with CGT and ESS. WPP and PV have high environmental and economic benefits, as well as high risks, so balancing the benefits and risks is the key to the optimal operation of the VPP.
- A basic scheduling model for the VPP operation is put forward without considering uncertainty. The maximum revenue of the VPP operation is taken as the objective function of the optimization model, considering energy balance constraints, different power sources, and system rotating reserve constraints. The basic scheduling results could provide an important decision-making reference for determining the VPP operation risks and verifying the effectiveness of the risk aversion model.
- A CVaR-robust-based aversion scheduling model for the VPP operation is constructed with the objective function of minimum operation losses. First, the uncertainty analysis for WPP, PV, SHS, and the load are made, and WPP and PV selected as the main uncertainty factors. Second, the conditional value at risk (CVaR) method and robust optimization theory are used to reflect the operation risks brought about by uncertainty in the objective function and restrictions, respectively. Finally, a solution methodology is constructed after converting the mixed integer nonlinear programming (MINLP) model into a mixed integer linear programming (MIP) model with three cases for comparative analysis.

The rest of this paper is organized as follows: Section 2 describes the basic structure of the virtual power plant, then, the output model of the power sources is introduced. Section 3 presents the basic scheduling model for the VPP under the objective function of the maximum operating revenue. Next, in Section 4, the uncertainty analysis is made and the risk aversion scheduling model is proposed based on the CVaR method and the robust optimization theory. Finally, Section 5 presents an industrial park group in northern China which was chosen as a simulation system for the verification of the effectiveness and applicability of the proposed scheduling model. Section 6 highlights the contributions and conclusions of the paper.

2. VPP Description

2.1. VPP Participants

This study integrated WPP, PV, SHS, CGT, ESS, and IBDR into the VPP. The energy scheduling of the VPP was mainly carried out by the energy management system (EMS). Based on the load demands of terminal users and the available outputs of different power sources, the optimal operation strategy of the VPP was established. Meanwhile, in order to fully motivate the user side to respond to the optimization scheduling, PBDR was implemented in this study, which could utilize time-of-use (TOU) prices to change the users' power consumption behavior and optimize the load curve. Moreover, assume the SHS was equipped with an annual regulating reservoir to improve the adjustment characteristics of the VPP, namely, the SHS could optimize the utilization of water storage according to the actual output of WP and PV, and participate in VPP optimization operation. IBDR was implemented through signing pre-agreements with the end users and providing a certain subsidy. When the content of the contract occurred, the scheduling agency could directly make the user adjust their power consumption behaviors to improve the power generation output or the spare output. Figure 1 is the basic structure of the virtual power plant.

In the VPP, WPP, PV, and CGT were the main power sources for satisfying the load demand. The surplus load demand was satisfied by SHS. The power generation of WPP and PV had great

uncertainty, but system was pre-scheduled. The determined scheduling plan for the VPP was needed before knowing the actual output. In order to overcome deviation from the scheduling plan, the ESS and CGT provided reserve services. IBDR users provided virtual power generation by changing their power consumption behaviors, and participated in power generation dispatching in the energy market and reserve market. Meanwhile, the SHS equipped with regulating reservoirs could also provide reserve services by changing its power generation plans. WPP and PV have great environmental and economic benefits, but the high uncertainty of these sources also brings high risks. Balancing the benefits and risks is a critical issue in the optimization of VPP operation.

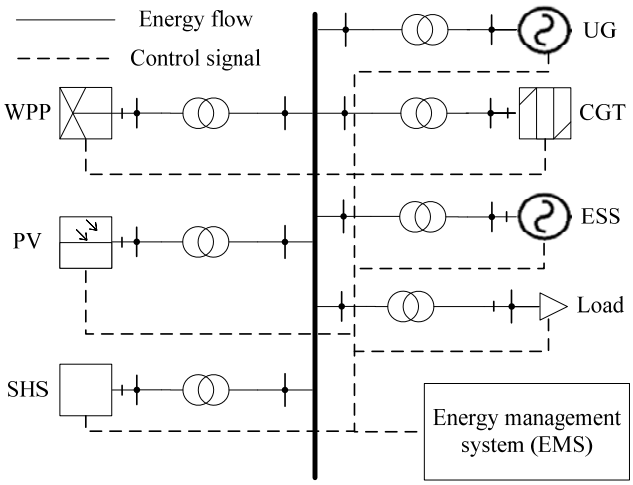

Figure 1. Basic structure of virtual power plant.

2.2. VPP Output Model

(1) WPP/PV output model

The output of the VPP was mainly derived from WPP, PV, SHS, ESS, and IBDR. Among these, the outputs of WPP and PV mainly depend on natural wind and solar irradiance, respectively, which have highly random outputs. Correspondingly, the outputs of WPP and PV have great uncertainty. Simulating wind speed and irradiance is the key to calculating the outputs of WPP and PV. The Rayleigh distribution function and beta distribution function have been proved that they could be used to simulate wind speed and solar irradiance. The output models of WPP and PV have already been constructed based on the simulation distribution function in our previous research [11]. The specific calculation process is not repeated here, Equations (1) and (2) calculate the available output of WPP and PV:

$$g^*_{WPP,t} = \begin{cases} 0, & 0 \le v_t < v_{in},\ v_t > v_{out} \\ \frac{v_t - v_{in}}{v_{rated} - v_{in}} g_R, & v_{in} \le v_t \le v_{rated} \\ g_R, & v_{rated} \le v_t \le v_{out} \end{cases}, \tag{1}$$

where $g^*_{WPP,t}$ is the available output of the WPP at time t. g_R is the rated output of the WPP. v_t is the real-time wind speed at time t. v_{in}, v_{out} and v_{rated} are the cut-in, cut-out, and rated speed of the WPP, respectively.

$$g^*_{PV,t} = \eta_{PV} \times S_{PV} \times \theta_t, \tag{2}$$

where $g^*_{PV,t}$ is the available output of PV at time t. η_{PV} and S_{PV} are the efficiency and total area of PV, respectively. θ_t is the solar radiation intensity at time t.

(2) SHS output model

In order to increase the regulation capacity of the VPP, this study selected the small hydropower generation system with annual adjustment reservoirs. SHS could ensure the hydropower output by adjusting the amount of water according to power demand considering the water level of the

adjustment reservoir. The output of a hydropower station mainly depends on the runoff and head height of the river. The expression is as follows:

$$g^*_{SHS,t} = \eta_{SHS} \times \rho \times Q_t \times H_t, \tag{3}$$

where $g^*_{SHS,t}$ is the available output of SHS at time t. η_{SHS} is the efficiency of the hydropower station's power generation. ρ is the gravitational acceleration of the SHS location. Q_t is the drainage of the SHS power generation at time t. H_t is the net head of hydropower station, $H_t = Z_u - Z_d$, where Z_u and Z_d represent the water levels in front of the dam and at the draft pipe outlet section, respectively. The actual output of the SHS mainly depends on the output limit of the hydropower unit, as follows:

$$g^*_{SHS,t} = \begin{cases} g^*_{SHS,t}, g^{\min}_{SHS} \le g^*_{SHS,t} \le g^{\max}_{SHS} \\ 0, g^*_{SHS,t} \le g^{\min}_{SHS} \end{cases}, \tag{4}$$

where $g^{\min}_{SHS}$ and $g^{\max}_{SHS}$ are the minimum and maximum outputs of the hydropower unit, respectively.

(3) IBDR output model

In IBDR, pre-agreements are generally signed with the users. When the response occurs, the users need to adjust their electricity consumption behaviors in accordance with the agreements, and receive financial compensation for this response. The IBDR program is mainly provided by demand response providers (DRPs). Because the revenue of DRPs is determined by the supply price of the demand response, DRPs participate in IBDR programs step-by-step according to the demand response (DR) price in accordance with the fluctuation of the electricity market price [34]. Figure 2 shows the step-wise DR price-demand curve.

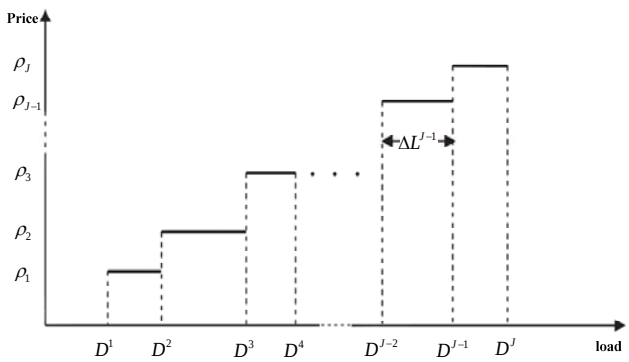

Figure 2. Step-wise DR price-demand curve.

According to Figure 2, the minimum required response for DRP i in step j is $D_i^{j,\min}$, and the corresponding maximum demand response is $D_i^{j,\max}$. Thus, DRPs need to meet the following principles when participating in energy market scheduling:

$$D_i^{j,\min} \le \Delta L_{i,t}^j \le D_{i,t}^j, j = 1, \tag{5}$$

$$0 \le \Delta L_{i,t}^j \le \left(D_{i,t}^j - D_{i,t}^{j-1}\right), j = 2, 3, \ldots, J, \tag{6}$$

$$\Delta L_{IB,t} = \sum_{i=1}^{I} \sum_{j=1}^{J} \Delta L_{i,t}^j, \tag{7}$$

where $\Delta L_{i,t}^j$ is the actual load reduction provided by DRP i in step j at time t. $D_{i,t}^j$ is the available load reduction provided by DRP i in step j at time t. $\Delta L_{i,t}$ is the cumulative load reduction provided by DRP i at time t. $\Delta L_{IB,t}$ is the output power provided by IBDR at time t.

(4) ESS operation model

The energy storage system unit participated in VPP power generation scheduling by utilizing its own charge and discharge characteristics. During the valley periods, energy storage was performed, and power generation was performed during the peak periods, to provide a reserve service for the VPP. This study introduced the state of charge (SOC) to reflect the remaining capacity of the ESS battery, which varies with the charge and discharge of the system, and is expressed as the percentage of the remaining battery power and its total capacity, as follows:

When the ESS is charging:

$$\mathrm{SOC}_{ESS,t} = \mathrm{SOC}_{ESS,t-1} + \eta^{ch} g^{ch}_{ESS,t} / \mathrm{C}_{ESS}, \tag{8}$$

When the ESS is discharging:

$$\mathrm{SOC}_{ESS,t} = \mathrm{SOC}_{ESS,t-1} - g^{dis}_{ESS,t} / \left(\eta^{dis} \mathrm{C}_{ESS}\right), \tag{9}$$

where $\mathrm{SOC}_{ESS,t}$ and $\mathrm{SOC}_{ESS,t-1}$ are the remaining capacities of the ESS battery at time t and t-1, respectively. η^{ch} and η^{dis} are the charge and discharge efficiencies of the ESS, respectively. $g^{ch}_{ESS,t}$ and $g^{dis}_{ESS,t}$ are the charge and discharge powers of the ESS at time t, respectively. C_{ESS} is the rated capacity of the ESS battery.

$$g_{ESS,t} = u^{ch} g^{ch}_{ESS,t} - u^{dis} g^{dis}_{ESS,t}, \tag{10}$$

$$g_{ESS,t} = \begin{cases} \Delta g_{NE,t}, -g^{ch,\max}_{ESS,t} \le \Delta g_{NE,t} \le g^{ch,\max}_{ESS,t} \\ -g^{dis,\max}_{ESS,t}, \Delta g_{NE,t} \le -g^{dis,\max}_{ESS,t} \\ g^{ch,\max}_{ESS,t}, \Delta g_{NE,t} \ge g^{ch,\max}_{ESS,t} \end{cases}, \tag{11}$$

where $g_{ESS,t}$ is the net charge and discharge power of ESS at time t, u^{ch} and u^{dis} are the charge and discharge state variables of ESS, respectively. When ESS is in the charge state, $u^{ch} = 1, u^{dis} = 0$, and when ESS is in the discharge state, $u^{ch} = 0, u^{dis} = 1$. $\Delta g_{NE,t}$ is the deviation of the outputs of WPP and PV, equal to $\left(g^{*}_{PV,t} - \overline{g}_{PV,t} + g^{*}_{WPP,t} - \overline{g}_{WPP,t}\right)$. $\overline{g}_{WPP,t}$ and $\overline{g}_{PV,t}$ are the actual available outputs of WPP and PV at time t, respectively. $g^{dis,\max}_{ESS,t}$ and $g^{ch,\max}_{ESS,t}$ are the maximum discharge and charging power values of the ESS at time t, respectively.

3. Basic Scheduling Model for VPP

3.1. Objective Function

In the power generation scheduling of a VPP including WPP, PV, and SHS, with the objective of maximum operating revenue, a basic mathematical model is constructed. The specific objective function is as follows:

$$\max N(\boldsymbol{g}_{VPP}) = R(\boldsymbol{g}_{VPP}) - C(\boldsymbol{g}_{VPP}), \tag{12}$$

where $\boldsymbol{g}_{VPP}$ is the output power of the VPP. $N(\cdot)$ is the net operating revenue of VPP. $R(\cdot)$ and $C(\cdot)$ are the operating income and cost of the VPP, respectively, as follows:

$$R(\boldsymbol{g}_{VPP}) = \sum_{t=1}^{T} \{R_{WPP,t} + R_{PV,t} + R_{SHS,t} + R_{CGT,t} + R_{ESS,t} + R_{IBDR,t}\}, \tag{13}$$

where $R_{WPP,t}$, $R_{PV,t}$, $R_{SHS,t}$, $R_{CGT,t}$, $R_{ESS,t}$ and $R_{IBDR,t}$ are the operating revenue of WPP, PV, SHS, CGT, ESS, and IBDR at time t, respectively. With the exception of ESS and IBDR, the revenue of the

generator sets is equal to the multiplier of the price and the amount of electricity. The operation revenue of ESS and IBDR are calculated as follows:

$$R_{ESS,t} = P^{dis}_{ESS,t} g^{dis}_{ESS,t} - P^{ch}_{ESS,t} g^{ch}_{ESS,t}, \tag{14}$$

$$R_{IBDR} = \sum_{i=1}^{I} \sum_{j=1}^{J} \Delta L^{j}_{i,t} P^{j}_{i,t}, \tag{15}$$

where $P^{dis}_{ESS,t}$ and $P^{ch}_{ESS,t}$ are the charge and discharge prices of the ESS at time t, respectively. $g^{dis}_{ESS,t}$ and $g^{ch}_{ESS,t}$ are the charge and discharge capacities of the ESS at time t, respectively. $P^{j}_{i,t}$ is the output price of DRP i in step j at time t. Furthermore, the operation cost of the VPP is mainly composed of CGT, SHS and ESS, the specific calculation is as follows:

$$C(g_{VPP}) = \sum_{t=1}^{T} \{C_{CGT,t} + C_{SHS,t}\}, \tag{16}$$

where $C_{CGT,t}$ and $C_{ESS,t}$ are the operation costs of CGT and ESS, respectively. Since the initial investment cost of the hydropower station is sunk cost, this study does not consider it, only considering the water cost in the operation phase. Therefore, the operation cost of the SHS is equal to the product of the water consumption and water price. Furthermore, the power generation cost of the CGT is mainly equal to the natural gas consumption cost and the startup-shutdown cost. The specific calculations are as follows:

$$C^{pg}_{CGT,t} = a_{CGT} + b_{CGT} g_{CGT} + c_{CGT} (g_{CGT,t})^2, \tag{17}$$

$$C^{ss}_{CGT,t} = [u_{CGT,t}(1 - u_{CGT,t})] \times \begin{cases} N^{hot}_{CGT}, T^{\min}_{CGT} < T^{\text{off}}_{CGT,t} \le T^{\min}_{CGT} + T^{cold}_{CGT} \\ N^{cold}_{CGT}, T^{\text{off}}_{CGT,t} > T^{\min}_{CGT} + T^{cold}_{CGT} \end{cases}, \tag{18}$$

where $C^{pg}_{CGT,t}$ is the natural gas consumption cost of the CGT at time t. $C^{ss}_{CGT,t}$ is the startup-shutdown cost of the CGT at time t. a_{CGT}, b_{CGT} and c_{CGT} are the cost coefficients of CGT power generation. The binary variable μ_{CGT} is the operation status of CGT at time t. N^{hot}_{CGT} and N^{cold}_{CGT} are the hot-startup and cold-startup costs of the CGT, respectively. $T^{\min}_{CGT}$ is the minimum allowable downtime of the CGT. T^{cold}_{CGT} is the cold-startup time of the CGT. $T^{\text{off}}_{CGT,t}$ is the continuous downtime of the CGT at time t.

3.2. Constraint Conditions

The optimization operation of the VPP followed a load supply and demand balance constraint, unit operation constraints, and system rotation reserve constraints. The specific constraints are as follows:

(1) Load supply and demand balance constraint:

$$\left\{ \underbrace{g_{WPP,t}(1 - \varphi_{WPP}) + g_{PV,t}(1 - \varphi_{PV}) + g_{CGT,t}(1 - \varphi_{CGT}) + u_{IB,t} \Delta L^{E}_{IB,t}}_{\text{VPP Power output in day ahead scheduling}} \right\} + g_{UG,t} \ge L^{0}_{t} - u_{PB,t} \Delta L_{PB,t}, \tag{19}$$

where $\Delta L^{E}_{IB,t}$ is the power for energy market scheduling provided by IBDR at time t. L^{0}_{t} is the power load demand of terminal users. The binary variables $u_{IB,t}$ and $u_{PB,t}$ are the statuses of IBDR and PBDR, respectively. Here, 1 means DR is implemented, and 0 means DR is not implemented. The load change produced by PBDR at time t is denoted by $\Delta L_{PB,t}$. According to the theory of microeconomics, PBDR is described by the demand-price elasticity as follows:

$$e_{st} = \frac{\Delta L_s / L_s^0}{\Delta P_t / P_t^0} \begin{cases} e_{st} \leq 0, s = t \\ e_{st} \geq 0, s \neq t \end{cases}, \tag{20}$$

where ΔL_s and ΔP_t are the changes in demand and price after PBDR, respectively. Then, the load change produced by PBDR can be calculated as:

$$\Delta L_{PB,t} = L_t^0 \times \left\{ e_{tt} \times \frac{\left[P_t - P_t^0\right]}{P_t^0} + \sum_{\substack{s=1 \\ s \neq t}}^{24} e_{st} \times \frac{\left[P_s - P_s^0\right]}{P_s^0} \right\}, \tag{21}$$

where L_t^0 and L_t are the load demands before and after PBDR, respectively. P_t^0 and P_t are the electricity prices before and after PBDR, respectively. e_{st} is the demand-price elasticity. When $s = t$, e_{st} is called self-elasticity, and when $s \neq t$, e_{st} is called cross-elasticity. The detailed mathematical description is provided in literature [6].

(2) SHS operation constraints

Small hydropower is constrained by season, due to the dry season and flood season. For the dry season, it is necessary to ensure that the water storage meets the night load; for the flood season, the water volume cannot exceed the maximum storage capacity, so it is necessary to adjust the water volume of the reservoir reasonably. Especially in the flood season, if the water volume of the reservoir has basically reached the maximum capacity, due to the maximum limit of the power generation drainage of the turbine unit, it is necessary to abandon the water to meet the reservoir storage requirements. Correspondingly, the reservoir water demand, power generation drainage, and water abandonment constraints are as follows:

$$V_{\min} \leq V_{T_0-1} + \int_{T_0-1}^{T_0} (q_t - Q_t - S_t) dt \leq V_{\max}, \tag{22}$$

$$Q_{\min} \leq Q_t \leq Q_{\max}, \tag{23}$$

$$S_{\min} \leq S_t \leq S_{\max}, \tag{24}$$

where V_{T_0-1} is the water demand of the regulating reservoir before the start of any power generation period. $V_{\min}$ is the minimum storage capacity that allows the reservoir to fall. $V_{\max}$ is the maximum water available to the reservoir. q_t, Q_t, S_t are the natural water supply the drainage of the hydropower station power generation and abandoned water flow of the hydropower station at time t, respectively. $Q_{\min}$ and $Q_{\max}$ are the minimum and maximum drainage of the hydropower station's power generation, respectively. $S_{\min}$ and $S_{\max}$ are the minimum and maximum allowed abandoned water for the SHS, respectively.

(3) IBDR operation constraints

IBDR can be applied for both energy market scheduling and reserve market scheduling. Thus, the detailed constraints of the IBDR operation are expressed as follows:

$$\Delta L_{IB,t}^E + \Delta L_{IB,t}^{up} \leq \Delta L_{IB,t}^{\max}, \tag{25}$$

$$\Delta L_{IB,t}^E + \Delta L_{IB,t}^{dn} \geq \Delta L_{IB,t}^{\min}, \tag{26}$$

where $\Delta L_{i,t}^j$ is the actual load reduction provided by DRP i in step j at time t. $\Delta L_{IB,t}^E$ is the scheduling power load change produced by IBDR in energy market scheduling. $\Delta L_{IB,t}^{up}$ and $\Delta L_{IB,t}^{dn}$ are the

scheduling power values of IBDR in the reserve market, represented by the upper and lower reserve outputs at time t, respectively. $\Delta L_{IB,t}^{\max}$ is the maximum output of IBDR at time t. $\Delta L_{IB,t}^{\min}$ is the minimum output of IBDR at time t. Similarly, IBDR must also meet the climbing constraints and startup-shutdown time constraints as follows:

$$u_{IB,t}\Delta L_{IB}^{-} \leq \Delta L_{IB,t} - \Delta L_{IB,t-1} \leq u_{IB,t}\Delta L_{IB}^{+}, \tag{27}$$

$$(T_{IB,t-1}^{\text{on}} - M_{IB}^{\text{on}})(u_{IB,t-1} - u_{IB,t}) \geq 0, \tag{28}$$

$$(T_{IB,t-1}^{\text{off}} - M_{IB}^{\text{off}})(u_{IB,t} - u_{IB,t-1}) \geq 0, \tag{29}$$

where ΔL_{IB}^{-} and ΔL_{IB}^{+} are the upper and lower climbing limits, respectively. $T_{IB,t-1}^{\text{on}}$ is the continuous operation time of IBDR at time $t-1$. M_{IB}^{on} is the minimum startup time of IBDR. $T_{IB,t-1}^{\text{off}}$ is the continuous downtime of IBDR at time t. M_{IB}^{off} is the minimum shutdown time of IBDR.

(4) System reserve constraints

$$g_{VPP,t}^{\max} - g_{VPP,t} + \Delta L_{PB,t} \geq r_1 \cdot L_t + r_2 \cdot g_{W,t} + r_3 \cdot g_{PV,t}, \tag{30}$$

$$g_{VPP,t} - g_{VPP,t}^{\min} \geq r_4 \cdot g_{W,t} + r_5 \cdot g_{PV,t}, \tag{31}$$

where $g_{VPP,t}^{\max}$ and $g_{VPP,t}^{\min}$ are the maximum and minimum available outputs of the VPP at time t, respectively. $g_{VPP,t}$ is the power generation output of the VPP at time t. $\Delta L_{PB,t}$ is the output provided by IBDR at time t. r_1, r_2 and r_3 are the upper rotation reserve coefficients of load, WPP, and PV, respectively. r_4 and r_5 are the lower rotation reserve coefficients of WPP and PV, respectively.

(5) Other constraints

For the VPP, the operation constraints of CGT, ESS, and PBDR should also be considered. Among these, the CGT is mainly needed to meet the maximum and minimum power constraints, startup-shutdown time constraints, and upper and lower climbing constraints. The ESS needed to meet the maximum charge-discharge power constraints, charge and discharge state constraints, etc. The output generated by PBDR also needed to meet the maximum output constraints, upper and lower climbing constraints and cumulative maximum output constraints at each moment. We have already constructed the constraints of CGT, ESS, and PBDR as shown in our previous research [32]; the paper did not display the model again.

4. Risk Aversion Model for VPP

4.1. Uncertainty Analysis

In the proposed VPP, four uncertainty factors exist, namely, $g_{WPP,t}$, $g_{PV,t}$, $g_{SHS,t}$ and L_t. Determining how to simulate the uncertainty factors and develop optimal strategies for the VPP is greatly important for decision makers. For the load demand, the load prediction deviation L_t^{e} could be described by a normal distribution function ($L_t^{\text{e}} \sim [0, \delta_{L,t}^2]$) [6], then, the distribution functions for load demand L_t could be obtained ($L_t \sim [L_t^{\text{f}}, \delta_{L,t}^2]$). For the day-ahead scheduling, since the daily weather forecasting technology is mature, and this study selected the small hydropower system with an annual regulating reservoir especially, the SHS output was adjustable and controllable in the short term. The proposed VPP included ESS and IBDR, so the reserve capability was sufficient, which could handle the load uncertainty adequately. Therefore, in this study, the impact of the load and SHS uncertainty on the VPP operation was not considered. Figure 3 shows the discretization method for the load demand distribution function.

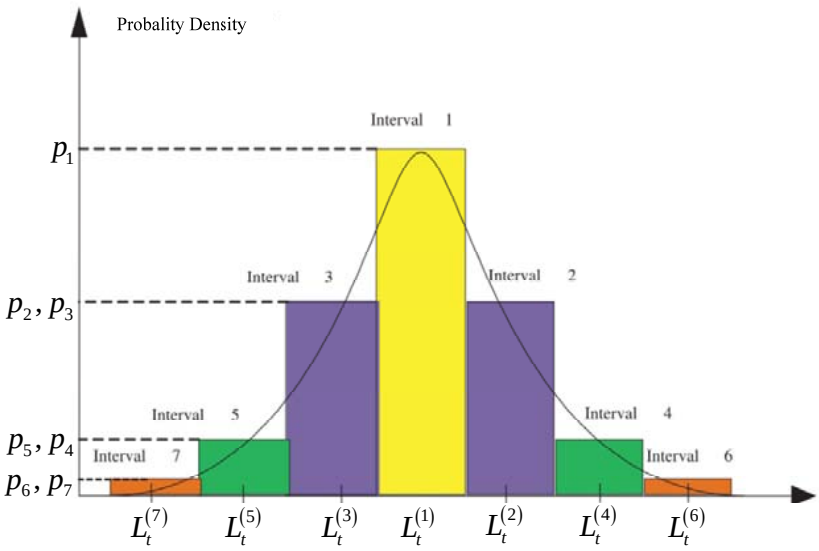

Figure 3. Discretization method of load demand distribution function.

Similarly, the existing researches prove that the Rayleigh distribution function and the beta distribution function could be used to describe natural wind speed and solar irradiance [21], respectively. Uncertainty factors could be simulated by the suitable probability distribution functions. However, three problems could not be ignored. First, the distribution functions for simulating uncertainty factors are continuous, but discretized distribution functions are needed for VPP scheduling. Deviation is inevitable, regardless of what discrete methods are used for the continuous distribution functions. Second, the parameters for the distribution functions are calculated by using vast historical data, which causes a great workload and reduced applicability. Third, uncertainty factors, especially in WPP and PV, have great randomness, and extreme situations are prone to happen. The distribution functions may be not useful. Therefore, a new risk aversion method was needed for VPP scheduling. Correspondingly, a CVaR-robust-based scheduling model is proposed for VPP optimal operation.

4.2. Mathematical Model

For the proposed model above, the uncertainty factors are distributed in the objective function and constraints. Determining how to describe the uncertainty factors was crucial to determining the optimal scheduling plan of the VPP. This paper proposes a risk aversion tool for the optimal operation of the VPP based on the CVaR method and the robust optimization theory.

4.2.1. CVaR Theory

In recent years, the financial sector has evolved a variety of risk analysis tools. Under normal market conditions and within a given confidence level, Value at Risk (VaR), which analyzes the risk characteristics quantitatively, can estimate the maximum possible loss of a portfolio over a specified period of time. However, VaR can only determine a risk situation under the given confidence level and doesn't consider the risk tail, so there are certain limitations in its practical applications. Conditional Value at Risk (CVaR) can describe the distribution of risk outside the confidence level. The basic principles are described as follows:

Set the portfolio vector as X and the random factor as random vector $\boldsymbol{Y} \in \boldsymbol{R}^m$ ($\boldsymbol{R}^m$ is the m-dimensional real space), the loss function of X can be expressed as $f(\boldsymbol{X}, \boldsymbol{Y})$; assume the joint probability density function of $\boldsymbol{Y}$ is $p(\boldsymbol{Y})$; for the determined X, the probability value of $f(\boldsymbol{X}, \boldsymbol{Y})$ caused by Y not exceeding the critical value α (α represents a particular loss level) is:

$$\psi(\boldsymbol{X},\alpha) = \int\limits_{f(\boldsymbol{X},\boldsymbol{Y})\leq\alpha} p(\boldsymbol{Y})d\boldsymbol{Y}, \tag{32}$$

where $\boldsymbol{X} \in \boldsymbol{\Omega}$, $\boldsymbol{\Omega}$ is a subset of the n-dimensional real space $\boldsymbol{R}^n$, representing the feasible set of the portfolio; $\psi(\boldsymbol{X},\alpha)$ is the loss accumulation distribution function under $\boldsymbol{X}$, which is the non-minus and the right-continuous of α.

According to Equation (32), the VaR and CVaR values of $f(\boldsymbol{X},\boldsymbol{Y})$ can be obtained when the confidence degree is β, which doesn't exceed the critical value α. The specific calculations are shown in Equations (33) and (34):

$$\alpha_\beta(\boldsymbol{X}) = \min\{\alpha \in \mathbf{R} : \psi(\boldsymbol{X},\alpha) \geq \beta\}, \tag{33}$$

$$\phi_\beta(\boldsymbol{X}) = \frac{1}{1-\beta}\int\limits_{f(\boldsymbol{X},\boldsymbol{Y})\geq\alpha_\beta(\boldsymbol{X})} f(\boldsymbol{X},\boldsymbol{Y})p(\boldsymbol{Y})d\boldsymbol{Y}, \tag{34}$$

where $\alpha_\beta(\boldsymbol{X})$ and $\phi_\beta(\boldsymbol{X})$ are the VaR value and CVaR value of the portfolio problem, respectively, where $\phi_\beta(\boldsymbol{X})$ is the CVaR value when the loss is greater than $\alpha_\beta(\boldsymbol{X})$. Since the analytic expression of $\alpha_\beta(\boldsymbol{X})$ is difficult to obtain, an approximate solution algorithm needs to be constructed by introducing a transformation function $F_\beta(\boldsymbol{X},\alpha)$ to substitute in for $\phi_\beta(\boldsymbol{X})$, the calculation of CVaR is simplified as follows:

$$F_\beta(\boldsymbol{X},\alpha) = \alpha + \frac{1}{1-\beta}\int\limits_{\boldsymbol{Y}\in\boldsymbol{R}^m} (f(\boldsymbol{X},\boldsymbol{Y})-\alpha)^+ p(\boldsymbol{Y})d\boldsymbol{Y}, \tag{35}$$

where $(f(\boldsymbol{X},\boldsymbol{Y})-\alpha)^+$ represents $\max\{f(\boldsymbol{X},\boldsymbol{Y})-\alpha, 0\}$. When the analytical expression $p(\boldsymbol{Y})$ is difficult to directly obtain, the integral term of Equation (35) is usually estimated by the historical data of Y or by the Monte Carlo simulation sample data. Set $Y_1, Y_2, \cdots, Y_N$ as N sample data of $\boldsymbol{Y}$, the estimated value of the function $F_\beta(\boldsymbol{X},\alpha)$ is:

$$\hat{F}_\beta(\boldsymbol{X},\alpha) = \alpha + \frac{1}{N(1-\beta)}\sum_{k=1}^{N}(f(\boldsymbol{X},\boldsymbol{Y})-\alpha)^+, \tag{36}$$

where $\hat{F}_\beta(\boldsymbol{X},\alpha)$ is the estimated value of $F_\beta(\boldsymbol{X},\alpha)$.

4.2.2. CVaR-Robust Model

Considering the risk brought about by the uncertainty factors to the VPP operation, the CVaR theory is applied to describe the scheduling operation risk of the VPP. According to Equation (12), set $\boldsymbol{G}^T = [g_{VPP,t}(1), g_{VPP,t}(2), \cdots, g_{VPP,t}(T)]$ as the decision vector, $\boldsymbol{y}^T = \left[\boldsymbol{g}_{WPP,t}, \boldsymbol{g}_{PV,t}, \boldsymbol{L}_t\right]$ is a multivariate random vector. The net operation revenue of the VPP is $N(\boldsymbol{G},\boldsymbol{y})$. Then, according to Equation (32), define the operation loss function of the VPP as $L(\boldsymbol{E},\boldsymbol{y}) = -N(\boldsymbol{E},\boldsymbol{y})$. The CVaR function of VPP scheduling considering uncertainty is characterized as follows:

$$F_\beta(\boldsymbol{E},\alpha) = \alpha + \frac{1}{1-\beta}\int\limits_{\boldsymbol{y}\in\boldsymbol{R}^m} (L(\boldsymbol{E},\boldsymbol{y})-\alpha)^+ p(\boldsymbol{y})d\boldsymbol{y}, \tag{37}$$

where α is the threshold value of the decision maker's risk judgment. β is the confidence degree of the VPP operation objective function. When Equation (36) reaches the minimum, namely the CVaR value, α is the VaR value. $g^*_{VPP,t}$ includes $g^*_{WPP,t}$, $g^*_{PV,t}$, $g^*_{CGT,t}$, $\Delta L^{E*}_{IB,t}$, $\Delta L^{up*}_{IB,t}$, $\Delta L^{dn*}_{IB,t}$. When $p(\boldsymbol{y})$ is difficult to determine, an approximate solution algorithm can be constructed, and the integral term of Equation (38) is usually estimated by the historical data of $\boldsymbol{y}$ or by the Monte Carlo simulation sample data. Set $y_1, y_2, \cdots, y_N$ as N sample data of $\boldsymbol{y}$, then the estimated value of the function $F_\beta(\boldsymbol{X},\alpha)$ is:

$$F_\beta(\boldsymbol{G},\alpha) = \alpha + \frac{1}{N(1-\beta)}\sum_{k=1}^{N}(L(\boldsymbol{E},\boldsymbol{y}) - \alpha)_k^+, \tag{38}$$

Second, apply the robust theory to convert the constraint conditions with uncertainty variables into stochastic constraint conditions by using the robust coefficient. Robust optimization theory is a mature theory that solves the problem of uncertain parameter optimization after multi-step stochastic optimization theory and fuzzy optimization theory [11]. This paper considers the uncertainty factors $g_{WPP,t}$ and $g_{PV,t}$, setting prediction deviations as $e_{WPP,t}$ and $e_{PV,t}$, then $g_{WPP,t}$ and $g_{PV,t}$ may fluctuate within $[(1-e_{WPP,t})\cdot g_{WPP,t}, (1+e_{WPP,t})\cdot g_{WPP,t}]$ and $[(1-e_{PV,t})\cdot g_{PV,t}, (1+e_{PV,t})\cdot g_{PV,t}]$. For ease of expression, $e_{RE,t}$ is used to replace $e_{WPP,t}$ and $e_{PV,t}$, and $g_{RE,t}$ is used to replace $g_{WPP,t}$ and $g_{PV,t}$. Correspondingly, $g_{RE,t}$ may fluctuate within $[(1-e_{RE,t})\cdot g_{RE,t}, (1+e_{RE,t})\cdot g_{RE,t}]$. Finally, calculate the system net load M_t as follows:

$$M_t = g_{CGT,t}(1-\varphi_{CGT}) + u_{IB,t}\Delta L_{IB,t}^E + g_{UG,t} - \left(L_t^0 - u_{PB,t}\Delta L_{PB,t}\right), \tag{39}$$

Then, Equation (19) could be rewritten as follows:

$$-\left[g_{RE,t}(1-\varphi_{RE}) \pm e_{RE,t}\cdot g_{RE,t}\right] \le M_t, \tag{40}$$

Equation (40) shows that the inequality constraint becomes stricter when the influence of the stochastic is greater. To ensure that the constraints meet the requirements when the actual output reaches the prediction boundary, an auxiliary variable $\theta_{RE,t}(\boldsymbol{\theta} \ge 0)$ is introduced to strengthen the above constraints. Assume $\theta_{RE,t} \ge |g_{RE,t}(1-\varphi_{RE}) \pm e_{RE,t}\cdot g_{RE,t}|$. Thus, Equation (40) can be changed as follows

$$-\left(g_{RE,t} + e_{RE,t}g_{RE,t}\right) \le -g_{RE,t} + e_{RE,t}|g_{RE,t}| \le -g_{RE,t} + e_{RE,t}\theta_{RE,t} \le M_t, \tag{41}$$

Equation (41) shows the most stringent robust constraints. Due the probability of the occurrence of an extreme scenario, we introduce the robust coefficients $\Gamma_{RE}, \boldsymbol{\Gamma} \in [0,1]$ to modify the above constraints as follows:

$$-\left(g_{RE,t} + e_{RE,t}g_{RE,t}\right) \le -g_{RE,t} + \Gamma_{RE}e_{RE,t}|g_{RE,t}| \le -g_{RE,t} + e_{RE,t}\theta_{RE,t} \le H_t, \tag{42}$$

Finally, Combining Equation (42) and Equations (20)–(31) with the objective function (Equation (38)), the stochastic optimization model could be constructed with a freely adjustable robust coefficient, as shown in Equation (43). The model can be used to calculate the optimization scheduling scheme with different robust coefficients considering the different risk attitudes of the policymakers.

$$\min F_\beta(\boldsymbol{G},\alpha) = \alpha + \frac{1}{N(1-\beta)}\sum_{k=1}^{N} z_k$$

$$s.t.\begin{cases} Eq.(20) - Eq.(31) \\ Eq.(37) - Eq.(43) \\ z_k = L(\boldsymbol{E},\boldsymbol{y}) - \alpha \\ z_k \ge 0 \\ other\ constriants \end{cases} \tag{43}$$

Overall, CVaR-robust-based scheduling can realize the safe and stable operation of the system within a certain disturbance range when the system's operation information is incomplete, improve the system's immunity to uncertainty factors, and achieve the scheduling target.

4.3. Solution Methodology

Equation (40) determines the objective function of the VPP risk aversion scheduling model, but it can be known from Equation (12) that the objective function contains a quad term, and is a mixed integer nonlinear programming (MINLP) problem. This problem is hard to solve and takes a lot of time, and it is difficult to achieve optimal results. Similarly, there are nonlinear constraints amongst the operation constraints of CGT units. The proposed objective function and constraints should be linearized before solving the model, which has also been researched in our previous work [11]. After the objective functions and constraints are linearized, the MINLP model will be converted to a mixed integer programming (MIP) model. Figure 4 is the solution flow chart of the proposed model.

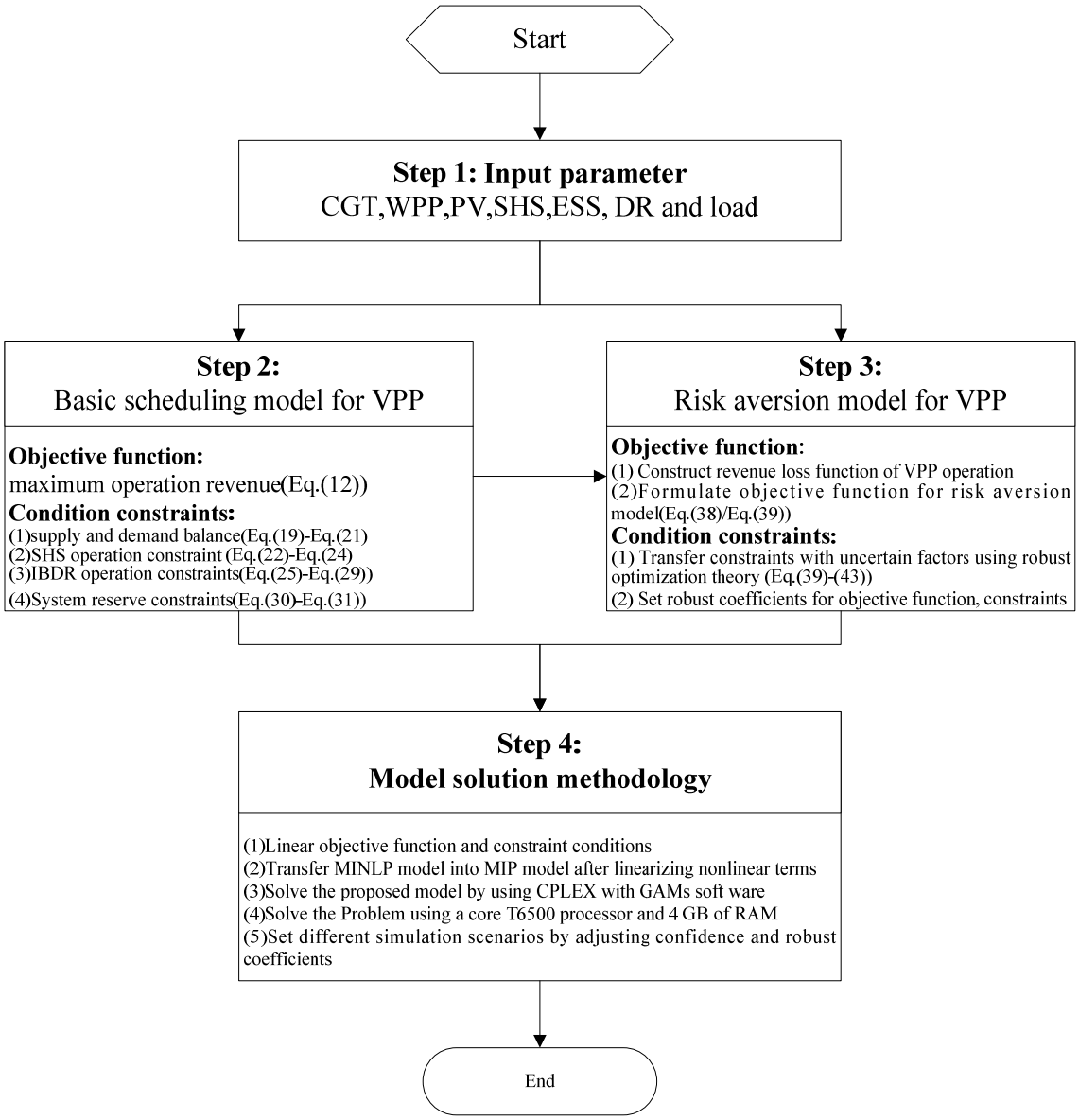

Figure 4. Solution flow of the proposed model.

Furthermore, in order to analyze the applicability of the proposed CVaR-robust method in solving the optimization operation of the VPP, this study set three simulation cases, namely, reference scenario, CVaR scenario and comprehensive scenario, and analyzed the effectiveness of the CVaR method and robust optimization theory in measuring and controlling the risks of VPP operation caused by uncertainties. These cases are described as follows:

Case 1: The reference scenario, using self-scheduling for the VPP without considering uncertainties. This scenario did not consider the uncertainty of WPP and PV. It analyzed the operational characteristics of different components in the VPP, and focused on the complementary effects between different components to obtain the optimal scheduling results for the VPP under the objective of maximizing operating revenue.

Case 2: The CVaR scenario, using self-scheduling for only the VPP with the CVaR method. This scenario focused on the uncertainty of WPP and PV in the objective function, and used the CVaR method to transform the objective function (Equation (37)). It analyzed the results of VPP operation under different confidence degrees, and verified the effectiveness of the CVaR method in dealing with wind and solar uncertainty.

Case 3: The comprehensive scenario, using self-scheduling for the VPP with the CVaR-robust method. This scenario further considered the influence of uncertainty factors on the operation of the VPP within constraints, and constructed random constraints (Equation (43)) by means of the robust optimization theory. The VPP scheduling optimization strategies under different robust coefficients and prediction accuracies were discussed, and the effectiveness of the CVaR-robust method was analyzed.

5. Case Analysis

5.1. Basic Data

An independent micro-grid located in an industrial park in East China (30°06′ N, 122°24′ E) was utilized for the simulation analysis of the proposed model. The park was equipped with two 0.25 MW WPPs, four 0.1 MW PVs, a 1 MW CGT, and a 0.2 MW·h ESS. An SHS was equipped with five small hydropower generating units of 50 kW each capacity, for which the annual average water flow was 40 m^3/h, and the maximum storage capacity was 936 m^3. The initial water volume of the reservoir was adjusted to 70% of the maximum capacity, and the price of water was set according to the literature [35]. The CGT predominantly selected was the G3406LE type gas turbine, with a rated output power of 1.025 MW, and a natural gas consumption of 107.7 m^3/h [11]. The startup and shutdown time of this gas turbine were 0.1 h and 0.2 h, respectively, and the startup-shutdown cost was about 95 ¥/MW·h. The gas cost of power generation could be described by a quadratic function, whose specific parameters were set according to [32]. Meanwhile, for an easy solution, the power generation cost function was linearized into two parts. The slope coefficients of the two parts were 105 ¥/MW and 355 ¥/MW, respectively, and the power generation loss of the unit was about 2.5%. The charging power of ESS did not exceed 0.04 MW, the discharge power did not exceed 0.05 MW [6], and the initial storage capacity of the ESS was 0. In addition, in order to ensure the safe and reliable operation of the energy storage, the ESS could not charge and discharge at the same time. Figure 5 is the load demand and available output on a typical load day.

Furthermore, in order to analyze the complementary effects between different power sources, the load data on a typical summer load day and on a typical winter load day were taken as input data. The maximum and minimum loads of the park were 0.9 MW and 0.709 MW in summer, respectively, and 0.879 MW and 0.737 MW in winter, respectively. According to [6], the cut-in, rated, and cut-out wind speeds of the WPP were set as 2.8 m/s, 12.5 m/s, and 22.8 m/s, respectively, and the shape parameter and scale parameter as $\varphi = 2$ and $\vartheta = 2\overline{v}/\sqrt{\pi}$, respectively. Referring to literature [32], it was assumed that the PV illumination intensity parameters ξ and ψ could be simulated as 0.3 and 8.54, respectively. The WPP and PV prediction errors were set to 5%. After getting the data of wind speed, radiation intensity, and load demand, through the scene simulation strategy of [11], one hundred sets of simulated scenes were generated, 10 typical scenarios were obtained according to the scenario reduction strategy in [6], and the average of each scenario result was taken as input data.

The on-grid prices of WPP, PV, SHS, and CGT in the park were 0.51 ¥/kW·h, 0.88 ¥/kW·h, 0.31 ¥/kW·h, and 0.42 ¥/kW·h, respectively. Meanwhile, in order to motivate the users to respond to the system's power generation scheduling, it was assumed that PBDR was implemented on the users'

side, and the terminal users' electricity price before PBDR was 0.59 ¥/kW·h. The price elasticity of the power demand was set according to literature [11]. The price in the flat period was unchanged; the price for the peak period was increased by 30%, and the price for the valley period was reduced by 50%. For IBDR, the energy price in the energy market was 0.45 ¥/kW·h, while the upper and lower rotation reserve prices in the reserve market were 0.25 ¥/kW·h and 0.55 ¥/kW·h, respectively. Meanwhile, in order to avoid excessive load fluctuations, which lead to the "peak-to-valley inversion" phenomenon, the load fluctuation caused by PBDR should not exceed ±0.04 MW [32], and the power output provided by IBDR should not exceed ±0.03 MW [32]. Table 1 shows the parameters of PBDR and IBDR.

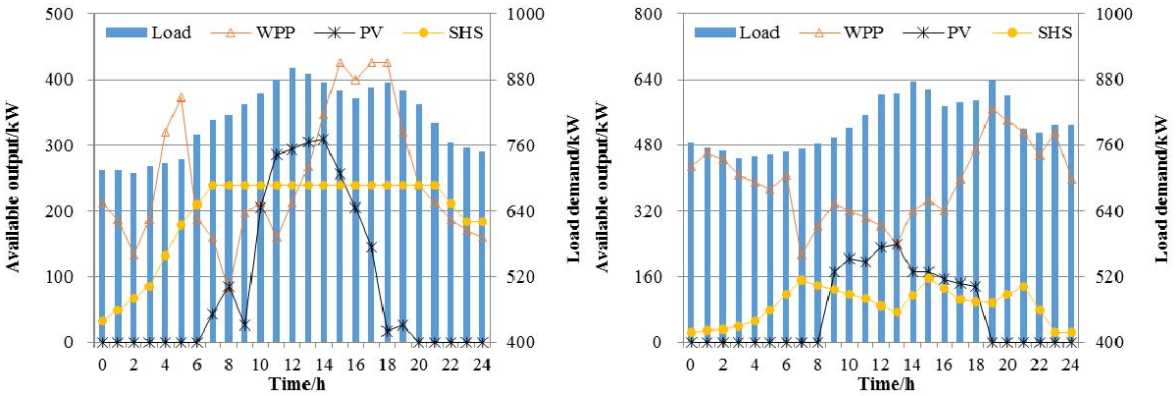

Figure 5. Load demand and available output on typical load day: (**left**) summer and (**right**) winter.

Table 1. Parameters of PBDR and IBDR in typical load day.

Time&price		PBDR			IBDR		
		Peak Period	Valley Period	Flat Period	Energy Market	Reserve Market Up	Reserve Market Down
Time divide	Summer	10:00−18:00	0:00−7:00	8:00−9:00&19:00−24:00			
	Winter	12:00−20:00	0:00−7:00	8:00−11:00&21:00−24:00			
Power price (¥/kW·h)		0.69	0.33	0.55	0.5	0.2	0.6

After taking inputs from the above basic data, the model was solved by the GAMS software using the CPLEX 11.0 linear solver from ILOG_solver [11]. The CPU time required for solving the problem of different case studies with a Lenovo IdeaPad Y450 series laptop computer powered by a core T6500 processor and 4 GB of RAM under these three cases is less than 20 s. When the optimization is MIP, the GAMs software obtains a satisfactory solution quickly.

5.2. Result Analysis

5.2.1. Scheduling Result of VPP in Case 1

This case focuses on the complementary effects of different power sources in the VPP, especially those between WPP, PV, and SHS. From the perspective of the load demand, on a typical winter day, due to the larger heating demand at night, the heating demand is relatively less during the daytime, so the peak-to-valley gap is lower. On a typical summer day, due to the higher cooling demand during the daytime, the cooling demand at night is relatively lower, so the peak-to-valley gap is relatively high. Figure 6 is the output distribution of VPP power generation in a typical day.

According to Figure 6, on the typical summer day, the main power sources for the load demand were CGT and SHS. The remaining load demand was satisfied by WPP. On the typical winter day, the main power sources were CGT and WPP. The remaining load demand was satisfied by SHS. This was due to the lower available output of WPP but higher available output of SHS and PV in summer, and lower available output of SHS and PV but higher available output of WPP in winter.

It can be seen that there were significant complementary effects between different power sources on the different typical days. The VPP could form a stable power output to meet the load demand by aggregating different distributed power sources, and could thus get the maximum operating revenue. Table 2 shows the scheduling results of VPP operation on the different typical load days.

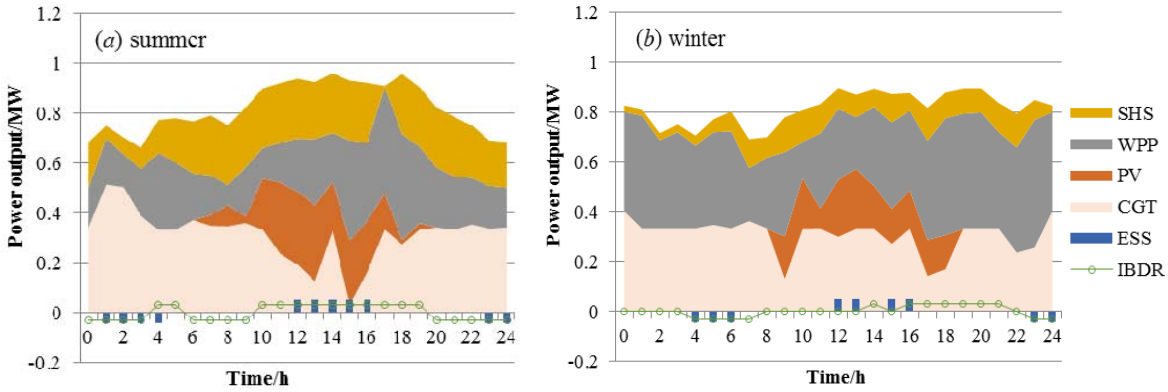

Figure 6. Output distribution of VPP power generation on typical day: (**a**) summer and (**b**) winter.

Table 2. Scheduling results of VPP operation in typical load day.

Typical Day	Power Output/MW·h						Abandoned Energy/MW·h			Revenue/¥
	CGT	PV	WPP	SHS	ESS	IBDR	WPP	PV	SHS	
Summer	7.562	2.09	5.517	4.652	(0.25, −0.24)	(0.36, −0.39)	0.48	0.11	0.245	7804.85
Winter	7.282	1.673	8.566	2.058	(0.20, −0.20)	(0.21, −0.18)	0.745	0.146	0.179	8265.32

According to Table 2, in order to maximize the operating revenue, the VPP prioritized the utilization of clean energy to meet the load demand. The total output of WPP, PV, and SHS was 12.259 MW·h on a typical summer day and 12.297 MW·h on the typical winter day. Correspondingly, the operating revenue of the VPP on the typical summer day was ¥460.47, which was lower than that of the typical winter day. Since the peak-to-valley ratio on the typical summer day was higher than that of the typical winter day, the outputs of CGT, ESS, and IBDR were also higher. Furthermore, the clean energy output and revenue of the VPP in different periods was analyzed. Figure 7 shows the power output and operating revenue of VPP in different load periods.

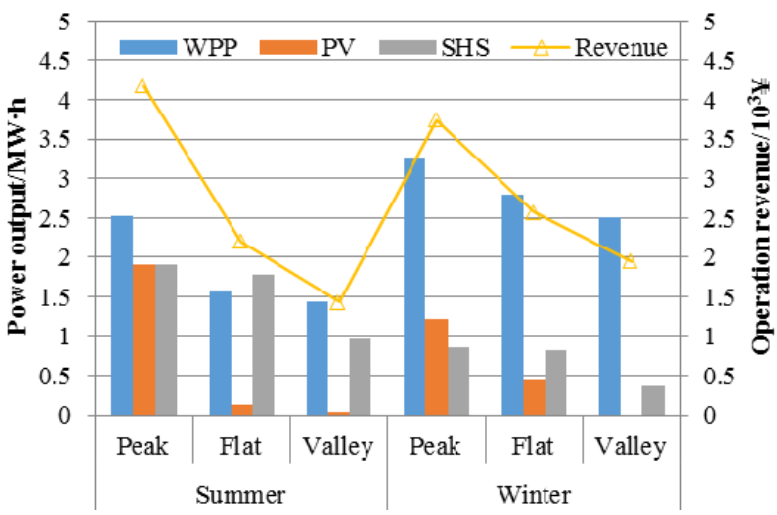

Figure 7. Power output and operation revenue of VPP in different load periods.

According to Figure 7, considering the different load periods, whether in summer or winter, the clean energy output in the peak load period was higher than that in other load periods. The outputs of WPP, PV, and SHS were 2.529, 1.91 and 1.915 MW·h, respectively. Correspondingly, the operating revenue was also high in the peak load period, at ¥4.175 × 10^3. Considering different power sources, the main clean energy outputs on the typical summer day were from PV and SHS, especially in the flat and valley periods. Take the valley period as an example; the outputs of PV and SHS were 0.137 and 1.777 MW·h, respectively. The main clean energy output on the typical winter day was from WPP, the outputs of PV were 3.273, 2.788 and 2.505 MW·h, in the three load periods, respectively. In total, the VPP could achieve the collaboration and complementarity of different distributed power sources in different load periods and seasons. The optimal operating revenue was obtained by maximizing the consumption of clean energy, and the optimal allocation of resources was realized.

5.2.2. Scheduling Result of VPP in Case 2

This scenario was mainly used to analyze the effectiveness of the CVaR method in measuring the uncertainty factor in the objective function. The initial confidence degree β was set to 0.9, and the optimal scheduling strategy of the VPP calculated. The respective total grid-connected outputs of WPP, PV, and SHS were 0.22, 0.417, and 0.242 MW·h for the typical summer day; and 0.123, 0.656 and 0.088 MW·h for the typical winter day, which were lower than those without considering uncertainty. The operating revenues of the VPP were ¥7645.5 on the typical summer day and ¥8137.68 on the typical winter day, which were lower than those without considering uncertainty. It can be seen that if the decision maker does not consider the uncertainty, the scheduling strategy of the VPP is arranged according to the risk neutral situation; when the actual output of WPP and PV deviates from the predicted results, the system will face a large operating risk. Figure 8 shows the output distribution of VPP power generation on typical load days.

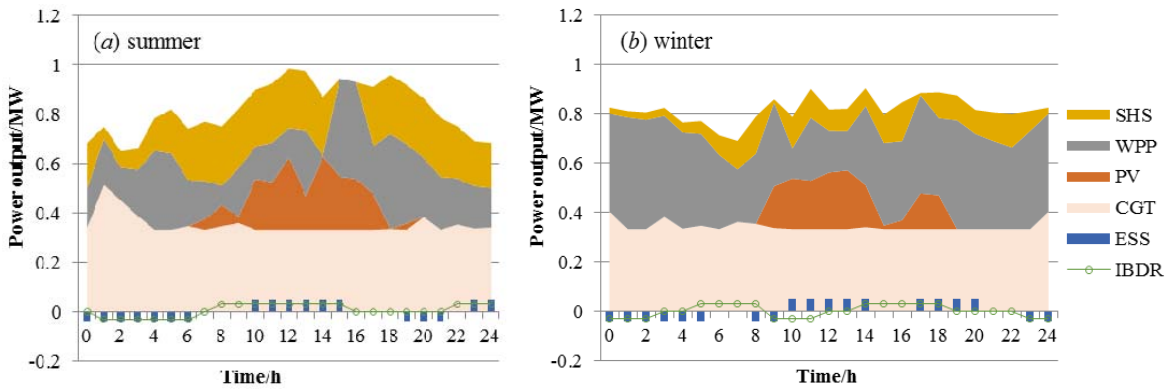

Figure 8. Output distribution of VPP power generation on typical load days in Case 2.

According to Figure 8, in order to avoid the uncertainty risk of WPP and PV, the VPP increased the power output of CGT. Compared with Case 1, the output of CGT was relatively stable, and the total output of CGT was higher, at 0.928 MW·h on the typical summer day and 0.908 MW·h on the typical winter day. Correspondingly, in order to provide sufficient reserve services for WPP and PV, the outputs of ESS and IBDR were also higher. In total, when considering uncertainty, the VPP reduced the output of WPP and PV, which lead to lower operating revenue, but could also avoid the risk of a power shortage penalty. In general, the confidence degree is a crucial parameter for balancing benefits and risks. A reasonable confidence degree guarantees the establishment of the optimal scheduling strategy of a VPP. Table 3 shows the scheduling results of VPP operation under different confidence degrees β in typical load day.

Table 3. Scheduling results of VPP operation under different confidence degrees β.

β	Summer							Winter						
	Power Output/MW·h						CVaR/¥	Power Output/MW·h						CVaR/¥
	CGT	PV	WPP	SHS	ESS	IBDR		CGT	PV	WPP	SHS	ESS	IBDR	
0.8	8.06	1.95	5.43	4.50	(0.3, −0.3)	(0.36, −0.30)	1764.58	7.61	1.61	8.43	2.01	(0.35, −0.33)	(0.33, −0.27)	1878.18
0.85	8.18	1.92	5.32	4.47	(0.35, −0.36)	(0.36, −0.24)	1740.27	7.80	1.59	8.26	2.00	(0.4, −0.36)	(0.30, −0.24)	1852.30
0.90	8.49	1.87	5.10	4.41	(0.4, −0.4)	(0.33, −0.18)	1725.59	8.19	1.55	7.91	1.97	(0.45, −0.44)	(0.27, −0.18)	1836.67
0.95	8.53	1.83	5.02	4.39	(0.5, −0.4)	(0.33, −0.15)	1713.89	8.31	1.51	7.79	1.96	(0.50, −0.48)	(0.27, −0.15)	1824.22
0.98	8.83	1.75	4.85	4.36	(0.5, −0.44)	(0.30, −0.15)	1703.36	8.67	1.45	7.53	1.95	(0.5, −0.48)	(0.24, −0.15)	1813.01

According to Table 3, the confidence degree β reflects the risk attitude of the decision maker. When β is high, the decision maker is the risk aversion type, who will reduce the scheduling of WPP and PV power generation outputs to avoid the operating risk of the VPP. Conversely, when β is low, the decision maker is the risk preference type, who will increase the scheduling of WPP and PV to capture excess economic returns. It can be seen that as β increased from 0.8 to 0.98, the output of clean energy power generation gradually reduced, and the output of CGT, ESS, and IBDR gradually increased. This shows that as the risk aversion of policy makers increases, the unit output of VPP that can provide reserve services gradually increases, correspondingly, the CVaR value is gradually reduced. Further, when the decision maker considers the uncertainty risk, WPP and PV bring different degrees of risk to the VPP operation due to different supply and demand relationships in different time periods, so the changes in the operating revenue of the VPP in different load periods and confidence degrees need to be analyzed. Figure 9 shows the revenue of the VPP operation under different β in different load periods.

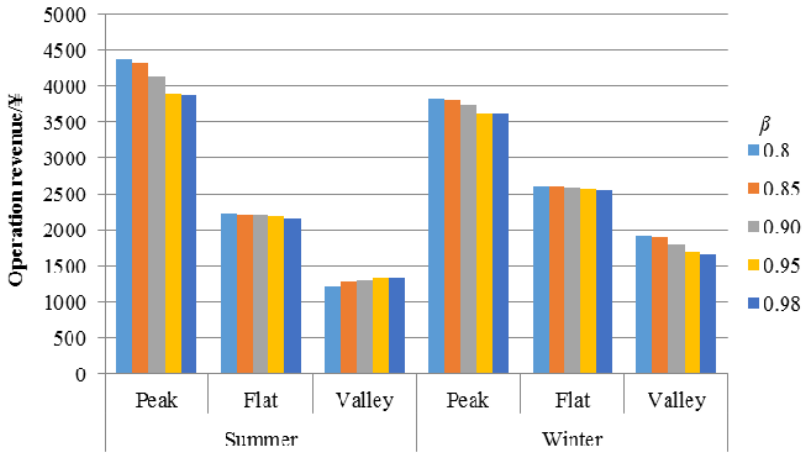

Figure 9. Revenue of VPP operation under different β in different load periods.

According to Figure 9, considering different time periods of the typical summer day, due to the heavy load during the peak period, the load supply and demand relationship was tight. So, when decision maker considered the uncertainty risk, the output of WPP and PV was significantly reduced, and the operating revenue significantly decreased with the increase of β. However, the supply and demand relationship in the valley period was not tight, so the dispatch of ESS and IBDR appropriately increased the grid-connected power of WPP and PV. For the typical winter day, the WPP's available output was higher at night, in order to avoid the risk to the VPP operation, the operating revenue in the valley period was significantly reduced with the increase of β. However, the ESS transferred part of the available output of WPP to the peak period. Correspondingly, the operating revenue did not decrease much in the peak period. In general, the CVaR method can measure the uncertainty factors in the objective function, reflect the risk attitude of the decision maker by setting the confidence degrees, and obtain the optimal operation strategy of the VPP.

5.2.3. Scheduling Result of VPP in Case 3

This subsection further discusses the impact of uncertainties on the VPP operation within constraints by introducing robust stochastic optimization theory. The initial robust coefficient Γ was set as 0.9, and the optimal scheduling strategy of the VPP calculated. The respective total grid-connected outputs of WPP, PV, and SHS were 4.797, 1.760 and 4.407 MW·h for the typical summer day; and 6.984, 1.455 and 1.901 MW·h for the typical winter day. The values of revenue, VaR and CVaR are 204.8 ¥, −68.71 ¥, −98.76 ¥, 343.7 ¥, −15.07 ¥, −38.81 ¥ lower than those in Case 2, respectively. It can be seen that when considering the uncertainties in the constraint conditions, the sensitivity of the decision maker to the risk will increase. In order to avoid risk to the VPP operation, the decision maker will

reduce the power generation of WPP and PV. Figure 10 shows the output distribution of VPP power generation on typical load days in Case 3.

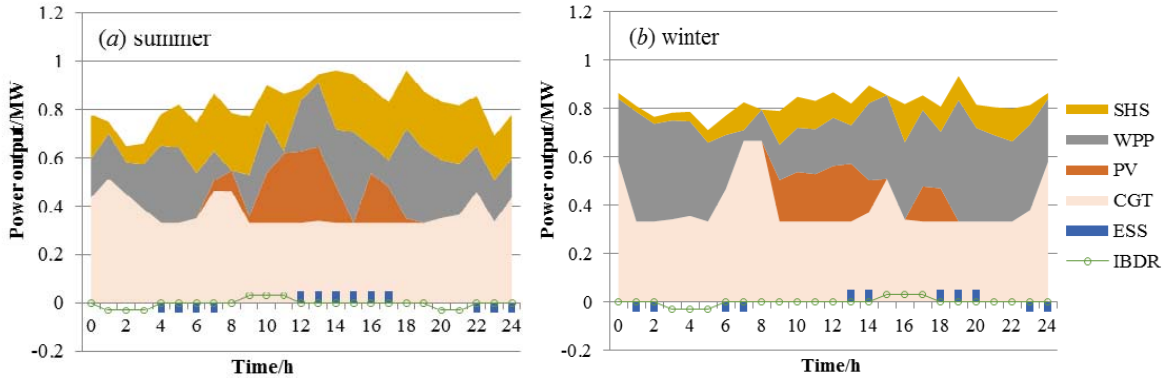

Figure 10. Output distribution of VPP power generation on typical load days in Case 3.

According to Figure 10, when the robust optimization theory was introduced, the VPP further compressed the grid-connected space of WPP and PV. Taking the typical summer load day as an example, the outputs of WPP and PV were reduced by 0.11 and 0.307 MW·h, respectively. However, the power generation output of the CGT was scheduled more by the VPP because it was more stable and controllable, and it increased by 0.431 MW·h. Since the power generation outputs of WPP and PV were reduced, the scheduling outputs of ESS and IBDR were eliminated as well. In the peak period, only, the ESS discharged, and the output of IBDR was reduced. In the valley period, the ESS charged and the output of IBDR increased. Table 4 shows the scheduling results of the VPP operation in different cases.

Table 4. Scheduling results of VPP operation in different Cases.

Typical Day		Power Output/MW·h						Operation Results/¥		
		CGT	PV	WPP	SHS	ESS	IBDR	Revenue	VaR	CVaR
Summer	Case 1	7.562	2.09	5.517	4.652	(0.25, −0.24)	(0.36, −0.39)	7804.85		
	Case 2	8.49	1.870	5.104	4.41	(0.40, −0.40)	(0.33, −0.18)	7645.50	1716.77	1725.59
	Case 3	8.921	1.760	4.797	4.407	(0.30, −0.28)	(0.09, −0.15)	7440.70	1785.48	1824.35
Winter	Case 1	7.282	1.673	8.566	2.058	(0.20, −0.20)	(0.21, −0.18)	8265.32	–	–
	Case 2	8.190	1.550	7.912	1.97	(0.45, −0.44)	(0.27, −0.18)	8137.68	1827.29	1836.67
	Case 3	9.342	1.455	6.984	1.901	(0.30, −0.24)	(0.09, −0.09)	7793.98	1842.36	1875.48

According to Table 4, the values of revenue, VaR, and CVaR in different cases are compared. When robust stochastic optimization theory was introduced into the conversion constraints with the uncertainty variable, the risk brought about by WPP and PV to the VPP could be better considered. The decision maker would further control the power generation of WPP and PV. Correspondingly, the operating revenue of the VPP also decreased, but the VaR and CVaR values increased under the same confidence degree β, indicating that the benefits and risks are interrelated, and the decision makers need to consider the corresponding risk while pursuing high economic returns. When decision makers want to avoid risk, they will need to discard some of the economic benefits. Furthermore, since the uncertainty in the constraints is described by the prediction error and the robustness coefficient, it can directly affect the optimal operation of the VPP, so sensitivity analysis was conducted between the prediction error $\boldsymbol{e}$, the robust coefficient Γ, and the confidence degree β, and the operation schemes of the VPP under different parameter combinations are discussed. Figure 11 shows the CVaR values of VPP operating under different robust coefficients.

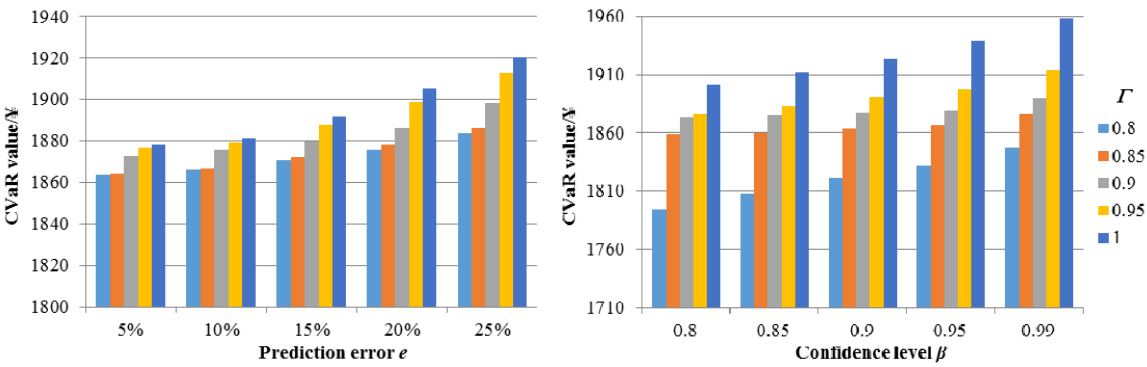

Figure 11. The CVaR values of VPP operation under different β, Γ and $\boldsymbol{e}$ (typical winter day).

According to Figure 11, the influence of prediction error $\boldsymbol{e}$ and robust coefficient Γ on the VPP operation is analyzed. When $\boldsymbol{e}$ was higher, the value of CVaR increased more than that when Γ increased by the same magnitude. When $\boldsymbol{e} \in [5\%, 10\%)$, the value of CvaR increased less than that when $\boldsymbol{e} \in [15\%, 25\%)$. It can be seen that when the prediction accuracy was reduced, the uncertainty factors brought higher risk to the VPP operation. Further, analyzing the effect of the robust coefficient Γ and confidence degree β on the VPP operation; when $\Gamma \leq 0.85$, increasing β lead to a great increase of CVaR, indicating that when decision makers consider uncertainty, the operation strategy of the VPP will change significantly. When $\Gamma \in (0.85, 0.95)$, the increase of β lead to a low increase of CVaR. At this time, the decision makers will balance the operating revenue and risk of VPP, so the decision scheme is relatively stable. Overall, the value of CVaR will increase with the increase of Γ. When $\Gamma \geq 0.95$, the growth of β brought a great increase of CVaR. At this time, decision makers are extremely risk aversion type. Small uncertainties will bring great operating risks. In order to achieve the optimal operation of a VPP, decision makers need to improve the accuracy of the uncertainty prediction, set a reasonable confidence degree and robust coefficient, take into account the risk and benefit of VPP operations, and formulate the optimal risk control strategy.

5.3. Comparative Analysis

The ESS could use its own charge and discharge capacity to optimize the distribution of WPP and PV power generation outputs, and PBDR could smooth the load demand curve through time-of-use prices, which both have important optimization effects on the VPP operation. On the other hand, the linearization process (proposed in Section 4.3) could reduce the time for solving the proposed model and improve the optimization degree of the scheduling results. Correspondingly, the paper mainly comparatively discusses the operation results of the VPP with and without the ESS under different peak-to-valley price gaps in this section.

5.3.1. The Impact of ESS on VPP Operation

The ESS could charge in the valley period and discharge in the peak period. So, it could not only improve the flexibility of the VPP operation, but also smooth the load demand curve, which is conducive to improving the grid-connected space of WPP and PV in the valley period and reducing the risks of WPP and PV to the VPP operation. In particular, WPP is the main clean energy output. This section selects the typical winter day and compares the operation results of the VPP with and without the ESS, as shown in Figure 12.

According to Figure 12, the power structure and operating revenue are compared before and after ESS. For the power structure, if the VPP did not contain ESS, the outputs of WPP, PV, and SHS were reduced by 0.078, 0.659 and 0.101 MW·h. However, the output of WPP and PV increased in peak period. This is because when the VPP did not contain ESS, WPP and PV was utilized more to meet the high load demand and obtain greater economic benefits. But in flat and valley periods, the VPP reduced the output of WPP and PV to avoid the uncertainty risk. For the operation results, the values

of revenue, VaR, and CVaR increased by −¥222.303, ¥71.641, and ¥69.315. During the peak period, the values increased by ¥227.30, ¥75.700, and ¥233.370. This is because when the VPP did not contain ESS, WPP and PV were difficult to store in peak periods. During the valley period, the outputs of WPP and PV were both reduced, resulting in a decrease in revenue and risk. In general, the ESS could utilize abandoned wind and solar energy for storage in the valley period, and release energy during the peak period, which was beneficial to alleviating the operating risk during the peak period, while improving the operating revenue of the VPP. Furthermore, the scheduling results of the VPP under different ESS capacities were measured. Table 5 shows the scheduling results of the VPP operation under different ESS capacities.

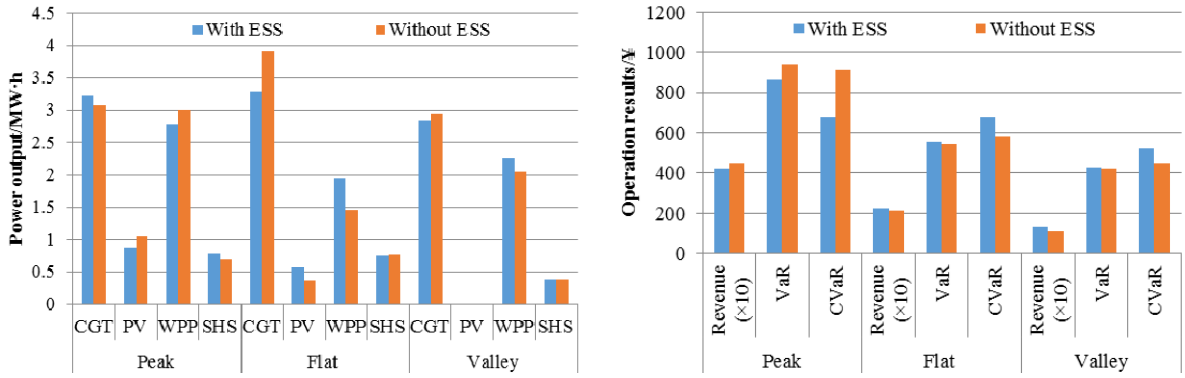

Figure 12. Operation results of VPP with/without ESS.

Table 5. Scheduling results of VPP operation under different ESS Capacities (typical winter day).

Capacity/MW·h	Power Output/MW·h						Operation Results/¥		
	CGT	PV	WPP	SHS	ESS	IBDR	Revenue	VaR	CVaR
0	9.941	1.419	6.517	1.834	0	(0.15, −0.15)	7645.54	1905.430	1938.840
0.2	9.342	1.455	6.984	1.901	(0.3, −0.24)	(0.09, −0.09)	7793.98	1842.362	1875.48
0.4	8.983	1.497	7.176	1.935	(0.36, −0.3)	(0.12, −0.12)	7867.843	1833.789	1869.525
0.6	8.682	1.539	7.316	1.965	(0.45, −0.39)	(0.12, −0.15)	7937.503	1822.579	1860.852
0.8	8.351	1.581	7.504	1.975	(0.51, −0.45)	(0.15, −0.18)	8028.115	1810.506	1851.539
1.0	8.199	1.602	7.599	1.982	(0.54, −0.48)	(0.15, −0.18)	8065.874	1795.140	1836.481

According to Table 5, when the ESS's capacity increased from 0 to 0.6 MW ((WPP, PV):ESS = 1.5:1), the values of revenue, VaR, and CVaR changed faster. When the capacity was higher than 0.6 MW, the value changed slower, which indicates that ESS could improve the grid-connected space of WPP and PV, but when the capacity was large enough, the ability to consume clean energy had basically reached the upper limit. At this time, other ways are needed to increase the output of WPP and PV with the objective of reducing the initial investment cost of the VPP and improving its operating revenue. Compared with the results when the capacity is 0, the outputs of WPP and PV increased by 1.082 and 0.183 MW·h, respectively, when capacity reached 1 MW·h. In general, with the increase of capacity, the operating revenue of the VPP increased, but the operating risk was improved as well. Hence, it is necessary to properly control the capacity of the ESS to balance the risks and benefits, which can ensure the optimal operation of the VPP.

5.3.2. The Impact of PBDR on VPP Operation

PBDR can motivate the terminal users to respond to the VPP operation schedule through time-of-use prices, and transfer partial load demand in the peak period to the valley period, which has an important effect on improving the grid-connected space of clean energy generation during the valley period, and relieving the supply-demand relationship during the peak period. Therefore, this study selected the typical summer day with a large peak-to-valley gap, analyzed the load demand curve before and after PBDR, compared the operation results of the VPP, and discusses the influences of

different peak-to-valley price gaps on VPP operation. Figure 13 shows the load demand of terminal customers in the typical day before/after PBDR.

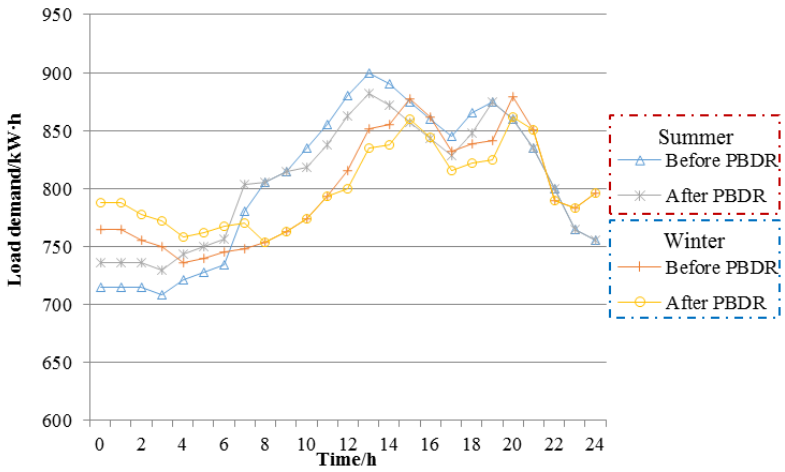

Figure 13. Load demand of terminal customers in typical day before/after PBDR.

According to Figure 13, the load demand curves before and after PBDR are compared. In a typical summer day, the maximum demands of the electrical load before and after PBDR were 0.900 and 0.882 MW, respectively. The minimum values were 0.709 and 0.730 MW. The peak-to-valley ratios of the load before and after PBDR in a typical summer day are 1.27 and 1.209. Similarly, the peak-to-valley ratios of the load before and after PBDR in a typical winter day are 1.194 and 1.144. It can be seen that PBDR is beneficial to reducing load demand in the peak period and increasing load demand in the valley period. Correspondingly, the flatter load demand curve also provides a greater grid-connected space for WPP and PV, which is beneficial to improving the operating revenue and reducing the operating risks of the VPP. Figure 14 shows the scheduling results of the VPP operating before and after PBDR.

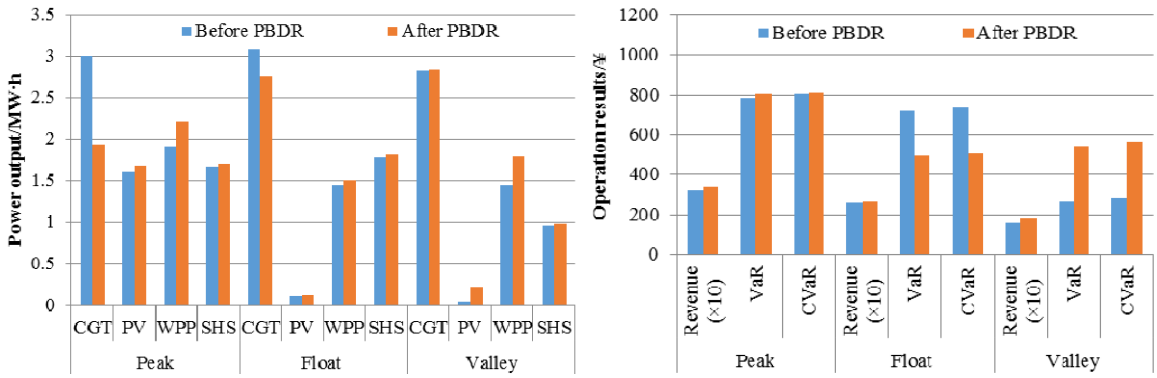

Figure 14. Operation results of VPP before/after PBDR.

According to Figure 14, the power structure and operation results before and after PBDR are compared. For the power structure, the output of WPP and PV after PBDR increased significantly, by 0.264 and 0.72 MW·h. Specifically, the output during the peak period and the valley period increased significantly. This is because the load curve after PBDR was smoother, and the reserve service space was larger during the peak period, and could support more grid-connected energy from WPP and PV. The increase of the load demand during the valley period also provided more grid-connected space for WPP and PV power generation. For the operation results, PBDR can smooth the load demand curves, the output of clean energy sources was more, correspondingly, and the revenue was also higher than that before PBDR. The operation revenue increased by ¥129.44, ¥40.62, and ¥262.74 in the three load

periods, but VaR and CVaR were reduced in the flat period, and increased in both the peak period and the valley period. This is because the clean energy output increased after PBDR, but the load during the flat period remained unchanged, while PBDR released more reserve service space, so the risk was reduced. During the peak period and the valley period, the output of clean energy increased, so the risk caused by uncertainty increased. Furthermore, the influence of the peak-to-valley price gap on VPP operation was analyzed. Table 6 shows the scheduling results of the VPP operation with different peak-to-valley price gaps.

Table 6. Scheduling results of VPP operation in different peak-to-valley price gaps.

Peak-to-Valley Price Gap	Load Demand/MW		Peak-to-Valley Ratio	Clean Energy Output/MW·h			Revenue/ ¥	VaR /¥	CVaR /¥
	Max	Min		PV	WPP	SHS			
1	0.900	0.709	1.270	1.76	4.797	4.407	7440.7	1785.48	1824. 35
2	0.891	0.723	1.233	1.848	5.037	4.440	7584.963	1805.447	1844.457
2.6	0.882	0.730	1.209	2.024	5.517	4.505	7873.49	1845.38	1884.67
3	0.878	0.733	1.197	2.141	5.837	4.549	8065.841	1872.002	1911.479
3.5	0.876	0.735	1.192	2.200	5.997	4.570	8162.017	1885.313	1924.883

According to Table 6, with the increase of the peak-to-valley price gap, the revenue space for VPP also increased. Correspondingly, the total output of WPP and PV increased significantly. When the peak-to-valley price gap was lower than 3, the values of revenue, VaR, and CVaR changed faster, but when the peak-to-valley price gap was higher than 3, these values changed slower. For the operating revenue and operating risk, the growth rate of revenue generated by PBDR was higher than that of the risk, which indicates that PBDR is conducive to improving the operating revenue and controlling the risk. Hence, in order to acquire the optimal operation, decision makers need to actively implement PBDR on the user side, set reasonable peak-to-valley price gaps according to the actual conditions, and encourage end users to respond to system energy scheduling, which can maximize economic benefits while minimizing operating risk.

5.3.3. The Impact of Linearization on VPP Operation

Quadratic terms exist in objective functions and a constraint condition, which results in the proposed model is a MINLP problems. However, the MINLP problem is complex, need much time to solve and hard to get the optimal solution. If the proposed model could be linearized, the above problem could be overcome. Figure 7 is the scheduling results of the VPP before/after linearizing model in typical summer day.

According to Table 7, the time for solving the model is lower in MIP model than that in MINLP model in three cases. This shows the linearization of the model will reduce the time for solving the model. Then, analyze the scheduling results in MIP model and MINLP model. Take Case 3 as example, the revenue is 135.25 ¥ lower in MIP model than that in MINLP model. However, the CVaR in MINLP is 80.77 ¥ higher than that in MIP model. This show the scheduling results could get more economic while rational controlling the operation risk after linearizing model. Overall, if the MINLP model is converted into MIP model, the optimization degree of the scheduling results is better.

Table 7. Scheduling results of the VPP before/after linearizing model in typical summer day.

cases	MIP			MINLP			Time/s	
	Revenue/¥	VaR/¥	CVaR/¥	Revenue/¥	VaR/¥	CVaR/¥	MINLP	MIP
Case 1	7804.85			7895.96			245 s	10 s
Case 2	7645.50	1716.77	1725.59	7442.65	1785.27	1893.48	278 s	14 s
Case 3	7440.70	1785.48	1824.35	7305.45	1805.45	1905.12	304 s	18 s

6. Conclusions

To make full use of the distributed energy on the user side, this study integrated WPP, PV, SHS, ESS, and IBDR into a VPP. Firstly, a basic scheduling model was constructed based on the maximum net operating revenue. Then, a risk aversion model for the VPP was put forward considering the uncertainty risk. The CVaR method was introduced to handle the uncertainty variables in constraint conditions, while robust optimization theory was used to convert the constraint conditions with uncertainty variables into stochastic constraint conditions. Third, a solution methodology was constructed after converting a MINLP model into MIP, and three cases were set for comparative analysis. Finally, an independent micro-grid on an industrial park in East China (30°06′ N, 122°24′ E) was utilized for a case study. The conclusions can be summarized as follows:

(1) The VPP could utilize the complementary characteristics of different distributed power sources to maximize the grid-connected electricity produced by clean energy sources. Because the peak-to-valley gap in summer is large, PV, SHS, and CGT were the main power sources, and especially, the SHS with annual regulation reservoirs could provide reserve services for WPP and PV. The peak-to-valley gap in winter is low, so WPP and CGT are the main power sources. ESS, IBDR, and CGT could provide reserve services for WPP and PV, which could fully utilize the clean energy and maximize the economic benefits to achieve the optimal operation of the VPP.

(2) The proposed risk aversion scheduling model for VPP operation, the CVaR method and robust optimization theory, could effectively handle operating risk brought about by uncertainty factors (WPP, PV). If considering uncertainty factors, the total respective outputs of WPP and PV were reduced by 0.33 and 0.72 MW·h on a typical summer day, and 0.218 and 1.582 MW·h on a typical winter day. This indicates that, if not considering uncertainty, the basic scheduling scheme would bring great risk to the system.

(3) The confidence degree and the robust coefficient were the key factors for establishing the optimal VPP operation scheme. When the prediction error $\boldsymbol{e}$ was higher, the value of CVaR increased more when Γ increased by the same magnitude, indicating that a lower prediction accuracy will amplify the uncertainty risk. When $\Gamma \geq 0.95$, decision makers were the extremely risk averse type, and smaller uncertainties would bring greater operating risks. When $\Gamma \leq 0.85$, less growth of β lead to a larger growth of CVaR. When $\Gamma \in (0.85, 0.95)$, the decision strategy was basically in a stable state, and the growth of β brought about the growth of CVaR, but the magnitude wais not large. It can be seen that decision makers need to improve the prediction accuracy and set reasonable confidence degrees and robust coefficients to obtain optimal risk control strategies.

(4) ESS and PBDR could smooth the load demand curve and provide greater grid-connected space for WPP and PV. When the VPP did not contain ESS, the output of WPP and PV was reduced by 0.078 and 0.659 MW·h in the typical winter day, respectively. When the capacity ratio of (WPP, PV):ESS was higher than 1.5:1, the values of revenue, VaR, and CVaR changed slower, which indicates that the ESS can improve the operating revenue of the VPP, but the capacity scale of the ESS should be controlled reasonably. The peak-to-valley ratio after PBDR was reduced from 1.27 to 1.209 in the typical summer day, but when the peak-to-valley price gap was higher than 3, the values of revenue, VaR, and CVaR changed slower, which indicates that a reasonable peak-to-valley price gap is beneficial to improving the grid-connected space of WPP and PV.

Author Contributions: L.J. (Liwei Ju) and proposed the researching framework. L.J. (Liwei Ju) and P.L. (Peng Li) conducted the empirical analysis and wrote the manuscript. Q.T. (Qinliang Tan), Z.F. (Zhongfu Tan) and G.D. (GejiriFu De) provided several useful recommendations on the manuscript revision.

Funding: This research was funded by Supported by the Beijing Social Science Fund (18GLC058, 16JDYJB044) and the Science Foundation of China University of Petroleum, Beijing (No. ZX20170256), the National Science Foundation of China (Grant No. 71273090) and the Beijing Social Science Fund (18GLC058).

Conflicts of Interest: The authors declare no conflict of interest.

References

1. Han, H.T.; Cui, H.T.; Gao, S.; Shi, Q.; Fan, A.; Wu, C. A Remedial Strategic Scheduling Model for Load Serving Entities Considering the Interaction between Grid-Level Energy Storage and Virtual Power Plants. *Energies* **2018**, *11*, 2420. [CrossRef]
2. Riccardo, I.; Benjamin, M.; Tetsuo, T. The Synergies of Shared Autonomous Electric Vehicles with Renewable Energy in a Virtual Power Plant and Microgrid. *Energies* **2018**, *11*, 2016.
3. Zhang, J.C.; Seet, B.C.; Lie, T.T. An Event-Based Resource Management Framework for Distributed Decision-Making in Decentralized Virtual Power Plants. *Energies* **2016**, *9*, 595. [CrossRef]
4. Liu, Z.Y.; Zheng, F.; Wang, L.; Zou, B.; Wen, F.; Xue, Y. Optimal Dispatch of a Virtual Power Plant Considering Demand Response and Carbon Trading. *Energies* **2018**, *11*, 1488. [CrossRef]
5. European Virtual Fuel Cell Power Plant Management Summary Report [EB/OL]. Available online: ftp://ftp.ee.polyu.edu.hk/zhaoxu/power%20system%20literature/euvpp.pdf (accessed on 13 August 2018).
6. Xie, J.; Cao, C. Non-Convex Economic Dispatch of a Virtual Power Plant via a Distributed Randomized Gradient-Free Algorithm. *Energies* **2017**, *10*, 1051. [CrossRef]
7. Ju, L.W.; Li, H.H.; Zhao, J.W.; Chen, K.; Tan, Q.; Tan, Z. Multi-objective stochastic scheduling optimization model for connecting a virtual power plant to wind-photovoltaic-electric vehicles considering uncertainties and demand response. *Energy Conver. Manag.* **2016**, *128*, 160–177. [CrossRef]
8. Dong, W.L.; Wang, Q.; Yang, L. A coordinated dispatching model for distribution utility and virtual power plants with wing/photovoltaic/hydro generators. *Autom. Electr. Power Syst.* **2015**, *39*, 75–82.
9. Wang, J.M.; Yang, W.H.; Chen, H.X.; Huang, L.; Gao, Y. The Optimal Configuration Scheme of the Virtual Power Plant Considering Benefits and Risks of Investors. *Energies* **2017**, *10*, 968–979. [CrossRef]
10. Project Interim Report [R/OL]. Available online: http://www.web2energy.com/ (accessed on 20 February 2013).
11. Ju, L.W.; Tan, Z.F.; Yuan, J.Y.; Tan, Q.; Li, H.; Dong, F. A bi-level stochastic scheduling optimization model for a virtual power plant connected to a wind–photovoltaic–energy storage system considering the uncertainty and demand response. *Appl. Energy* **2016**, *171*, 184–199. [CrossRef]
12. Pang, Z.H.; Kong, Y.L.; Pang, J.M.; Hu, S.; Wang, J. Geothermal Resources and Development in Xiongan New Area. *Bull. Chin. Acad. Sci.* **2017**, *32*, 1224–1230.
13. Can Kao Xiao Xi. Available online: http://www.cankaoxiaoxi.com/china/20170524/2034700.shtml (accessed on 24 May 2017).
14. National Development and Reform Commission. Available online: http://www.ndrc.gov.cn/gzdt/201608/t20160818_815086.html (accessed on 5 August 2016).
15. Muhammad, F.Z.; Elhoussin, E.; Mohamed, B. Microgrids energy management systems: A critical review on methods, solutions, and prospects. *Appl. Energy* **2018**, *222*, 1033–1055.
16. Aboelsood, Z.; Hossam, A.G.; Ahmed, E. Optimal planning of combined heat and power systems within microgrids. *Energy* **2015**, *93*, 235–244.
17. Bai, H.; Miao, S.H.; Ran, X.H.; Ye, C. Optimal Dispatch Strategy of a Virtual Power Plant Containing Battery Switch Stations in a Unified Electricity Market. *Energies* **2015**, *8*, 2268–2289. [CrossRef]
18. Cao, C.; Xie, J.; Yue, D.; Huang, C.; Wang, J.; Xu, S.; Chen, X. Distributed Economic Dispatch of Virtual Power Plant under a Non-Ideal Communication Network. *Energies* **2017**, *10*, 235. [CrossRef]
19. Liu, Y.Y.; Li, M.; Lian, H.B.; Tang, X.; Liu, C.; Jiang, C. Optimal dispatch of virtual power plant using interval and deterministic combined optimization. *Inter. J. Electr. Power Energy Syst.* **2018**, *102*, 235–244. [CrossRef]
20. Faeze, B.; Masoud, H.; Shahram, J. Optimal electrical and thermal energy management of a residential energy hub, integrating demand response and energy storage system. *Energy Build.* **2015**, *90*, 65–75.
21. Mashhour, E.; Moghaddas, M.S. Bidding strategy of virtual power plant for participating in energy and spinning reserve markets: Part I problem formulation. *IEEE Trans. Power Syst.* **2011**, *26*, 949–956. [CrossRef]
22. Tascikaraoglu, A.; Erdinc, O.; Uzunoglu, M.; Karakas, A. An adaptive load dispatching and forecasting strategy for a virtual power plant including renewable energy conversion units. *Appl. Energy* **2014**, *119*, 445–453. [CrossRef]
23. Mohammadi, J.; Rahimikian, A.; Ghazizadeh, M.S. Aggregated wind power and flexible load offering strategy. *IET Renew. Power Gener.* **2007**, *5*, 439–447. [CrossRef]

24. Shayeghi, H.; Sobhani, B. Integrated offering strategy for profit enhancement of distributed resources and demand response in microgrids considering system uncertainties. *Energy Convers. Manag.* **2014**, *87*, 765–777. [CrossRef]
25. Shropshire, D.; Purvins, A.; Papaioannou, I.; Maschio, I. Benefits and cost implications from integrating small flexible nuclear reactors with offshore wind farms in a virtual power plant. *Energy Policy* **2012**, *46*, 558–573. [CrossRef]
26. Riveros, J.Z.; Bruninx, K.; Poncelet, K. Bidding strategies for virtual power plants considering CHPs and intermittent renewables. *Energy Convers. Manag.* **2015**, *103*, 408–418. [CrossRef]
27. Hrvoje, P.; Juan, M.; Antonio, J.C.; Kuzle, I. Offering model for a virtual power plant based on stochastic programming. *Appl. Energy* **2013**, *105*, 282–292.
28. Heredia, F.J.; Rider, M.J.; Corchero, C. Optimal bidding strategies for thermal and generic programming units in the dayahead electricity market. *IEEE Trans. Power Syst.* **2010**, *25*, 1504–1518. [CrossRef]
29. Peik-Herfeh, M.; Seifi, H.; Sheikh-El-Eslami, M.K. Decision making of a virtual power plant under uncertainties for bidding in a day-ahead market using point estimate method. *Int. J. Electr. Power Energy Syst.* **2013**, *44*, 88–98. [CrossRef]
30. Yang, H.M.; Yi, D.X.; Zhao, J.H.; Luo, F.; Dong, Z. Distributed optimal dispatch of virtual power plant based on ELM transformation. *Management* **2014**, *10*, 1297–1318. [CrossRef]
31. Zamani, A.G.; Zakariazadeh, A.; Jadid, S. Day-ahead resource scheduling of a renewable energy based virtual power plant. *Appl. Energy* **2016**, *169*, 324–340. [CrossRef]
32. Tan, Z.F.; Wang, G.; Ju, L.W.; Tan, Q.; Yang, W. Application of CVaR risk aversion approach in the dynamical scheduling optimization model for virtual power plant connected with wind-photovoltaic-energy storage system with uncertainties and demand response. *Energy* **2017**, *124*, 198–213. [CrossRef]
33. Morteza, S.; Mohammad-Kazem, S.; Mahmoud-Reza, H. An interactive cooperation model for neighboring virtual power plants. *Appl. Energy* **2017**, *200*, 273–289.
34. Ju, L.W.; Tan, Z.F.; Li, H.H.; Tan, Q.; Yu, X.; Song, X. Multi-objective operation optimization and evaluation model for CCHP and renewable energy based hybrid energy system driven by distributed energy resources in China. *Energy* **2016**, *111*, 322–340. [CrossRef]
35. Yang, Q.; Yuan, Y.; Wang, M.; Zhou, J.; Bao, J.; Zhang, C. Optimal capacity configuration of standalone hydro-photovoltaic-storage microgrid. *Electr. Power Autom. Equip.* **2015**, *35*, 37–44.